designs

MDPI

Article

A Dynamic Matrix for the Study of Free Vibrations of Thin Circular Cylindrical Shells under Different Boundary Conditions

Marco Cammalleri * and Antonella Castellano

Department of Engineering, University of Palermo, 90128 Palermo, Italy; antonella.castellano@unipa.it
* Correspondence: marco.cammalleri@unipa.it

Abstract: Although free vibrations of thin-walled cylinders have been extensively addressed in the relevant literature, finding a good balance between accuracy and simplicity of the procedures used for natural frequency assessment is still an open issue. This paper proposes a novel approach with a high potential for practical application for rapid esteem of natural frequencies of thin-walled cylinders under different boundary conditions. Starting from Donnell–Mushtari's shell theory, the differential problem is simplified by using the principle of virtual work and introducing the flexural waveforms of a beam as constrained as the cylinder. Hence, the formulation is reduced to the eigenvalue problem of an equivalent 3×3 dynamic matrix, which depends on the cylinder geometry, material, and boundary conditions. Several comparisons with experimental, numerical, and analytical approaches are presented to prove model reliability and practical interest. An excellent balance between fast usability and accuracy is achieved. The user-friendliness of the model makes it suitable to be implemented during the design stage without requiring any deep knowledge of the topic.

Keywords: thin-walled cylinder; free vibrations; natural frequencies; eigenvalue problem; closed-form solution

Citation: Cammalleri, M.; Castellano, A. A Dynamic Matrix for the Study of Free Vibrations of Thin Circular Cylindrical Shells under Different Boundary Conditions. *Designs* **2023**, *7*, 122. https://doi.org/10.3390/designs7060122

Academic Editor: José António Correia

Received: 30 August 2023
Revised: 6 October 2023
Accepted: 22 October 2023
Published: 26 October 2023

1. Introduction

Thanks to their light weight and structural efficiency, cylindrical shells have been used in several engineering applications, ranging from pressure vessels, piping systems, and heat exchangers to the latest employment in the aerospace industry, such as aircraft fuselage and rocket bodies. Besides developing mathematical models to address the mechanical behaviour of thin-walled cylinders under static loads, characterising their dynamic response to free vibrations has attracted researchers' interest since the nineteenth century, intending to predict their natural frequencies already during the design stage to prevent time-varying loads from causing severe faults during the manufacturing process or normal use [1,2].

The first theories on the elastic behaviour of homogeneous and isotropic cylindrical shells that have laid the basis for the natural vibrations analysis were proposed by Love [3], Flügge [4], Timoshenko [5], Sanders [6], Reissner [7], Donnell [8], and Mushtari [9]. In a monography of 1973, Leissa [10] reviewed the state of the research on the vibrations of shells up to that point. Flügge [4] was the first to find exact solutions for natural frequencies of shells of infinite length with simply supported ends. Flügge's approach was used by Arnold and Warburton [11], who instead used Timoshenko's equations and proposed some of the first experimental results of simply supported thin cylinders. Nonetheless, this was the only possible exact solution that could be solved before the advent of high-speed digital calculators. For instance, Warburton [12] discussed an exact general theory to determine natural frequencies for cylindrical shells with any end conditions. Still, it is unsuitable for rapid estimates since it is based on an iterative approach requiring the reasonable assumption of an initial natural frequency. Indeed, due to the continuous nature of the

problem, finding the exact eigenfunctions by integrating the equations of motion, which constitute a system of partial differential equations, is far from trivial.

Therefore, some early approximated approaches based on energy minimisation were proposed, such as the Rayleigh–Ritz method [13] that relies on Lagrange's equations written for displacements in the three fundamental directions, i.e., the axial, circumferential, and radial, after the assumption of a reasonable waveform as eigenfunction. According to Rayleigh's principle, Arnold and Warburton [14] proved that performing a variables separation in the eigenfunctions and introducing the beam flexural waveform in the vibrational displacements for clamped-ended and simply supported cylinders results in simplified calculation and yet rather accurate results. Sewall and Naumann [15] provided experimental and analytical results obtained by a similar approach. Koval and Cranch [16] and Smith and Haft [17] focused their works on the clamped/clamped cylinders from an experimental and numerical point of view, respectively. Among the contributions of the second half of the twentieth century, it is worth mentioning the research of Sharma on the free vibration of clamped/free cylinders based on an iterative approach derived from Flügge's equations [18] and an approximated closed-form solution derived from Sanders' equations based on Rayleigh's approach starting from the vibrational mode of a cantilever beam [19].

After the first pioneering studies on the natural vibration of thin cylindrical shells, it became clear that a trade-off between accuracy and fast calculation was necessary to integrate the partial differential equations underpinning the problem of free vibrations of cylinders with any boundary condition [20–22]. In 1966, Forsberg [23] compared three methods to predict the natural frequencies of thin cylinders: an exact solution, a finite difference solution, and an energetic approach. The latter was the only one yielding an explicit expression.

The rapid development of high-speed automatic calculators over the last decades has fostered the introduction of new algorithms to solve the free vibrations problem of thin circular cylindrical shells iteratively or numerically [24]. Chung [25] obtained the expression of the frequency equation for any boundary condition using Sanders' shell equations with the axial displacements represented as Fourier series, but an iterative numerical method is required. Bert and Malik [26] proposed a semi-analytical approach based on the differential quadrature method applied to Flügge's equations, while Loy et al. [27] presented an improved version of the same algorithm. Still, in both cases, a convergence analysis is necessary. Zhang et al. [28] used the local adaptive differential quadrature method, which employs localised interpolating basis functions and exterior grid points for boundary treatments. Pellicano [29] proposed a method for analysing linear and nonlinear vibrations of circular cylindrical shells with different boundary constraints, using harmonic functions and Chebyshev polynomials for displacements and a numerical technique for the resolution. Xuebin [30] used variables separation for any boundary conditions and applied the Newton–Raphson iteration method to solve a coupled polynomial eigenvalue problem based on Flügge's equations. Khalili et al. [31] formulated a 3D refined higher-order shear deformation theory for the free vibration analysis of simply supported and clamped-ended cylindrical shells; the solution was obtained by the Galerkin numerical method. Xie et al. [32] used the Haar wavelet discretisation method. Xing et al. [33] presented an exact solution for different constraints from Donnell–Mushtari's equations using variables separation and Newton's iterative method. A similar approach was used by Fakkaew et al. [34]. Lastly, the latest contributions focus on the finite element method (FEM) using the block Lanczos iteration method [35], the reverberation-ray matrix approach [36], Galerkin projections of the partial differential equations governing the shell equations of motion [37], the symplectic approach [38,39], and the isogeometric analysis [40] to extend the theory of natural vibrations to various thin-walled structures, also in composite materials [41].

The reduction or even absence of simplifying assumptions in the above numerical methods yields more accurate solutions. Nevertheless, the calculation procedure is often

cumbersome: adequate knowledge of the employed numerical method is required to ensure the algorithm convergence, and the computing process may be computationally intense and time-consuming, sometimes requiring a first-attempt solution reasonably close to the unknown exact one. As a result, higher accuracy is achieved at the expense of usability and immediacy. Therefore, simplified approaches leading to more straightforward explicit formulations are still deemed worthy of investigation, not only for the free vibration problem, but also in other analysis of the dynamic stability, e.g., the vibration buckling problem of shells under pulsating external loads [42–44]. Moreover, the solution achieved through a simplified rapid procedure can be used as the initial guess value for the numerical methods.

The simplifying assumptions can concern the formulation of the equations of motion for thin cylinders [8,9,45–49] or the approach for solving the partial differential equations by using energetic methods such as Rayleigh–Ritz's [50,51] or Hamilton's principle [46,48,52] and introducing the beam flexural vibrations in the displacements eigenfunctions for thin cylinders [10,14,15,20,21,45–47,53–55]. However, despite the simplification, a closed-form solution is not always ensured [48,51]. Moreover, a more immediate mathematical treatment is achieved at the expense of accuracy, which should be ensured within practical thresholds [23]. Nonetheless, these authors believe that a practical and fast explicit formulation is vital to predict the natural frequencies of thin-walled cylinders in various boundary conditions with sufficient accuracy and without requiring deep expertise on the topic, which is clearly rather challenging, so as to be easily integrated into a wider research framework. For instance, the approximated closed-form solution for clamped-ended cylinders addressed in [46] and based on a series of cascaded equations derived from the application of Hamilton's principle to Love's equations have been exploited as a starting point for later more complex studies to analyse a cylindrical shell containing a variably oriented semi-elliptical surface crack [56] and the transient elastodynamic behaviour of cylindrical tubes under moving pressures [57].

Hence, this paper proposes a novel, straightforward, closed-form solution for the natural vibrations of thin cylindrical shells with different boundary conditions. The main scope is to provide scholars and engineers with an easy-to-use mathematical tool which, to the authors' knowledge, is not yet available in the relevant literature. Starting from Love's theory, the equations of motion are approximated by Donnell–Mushtari's assumptions and introduced in the principle of virtual work. After normalising the resulting system to the cylinder length, the eigenfunctions of displacements are assumed as separate-variables functions of the corresponding flexural waveform of a beam subject to the same constraints. The final mathematical formulation is reduced to the eigenvalue problem of a 3×3 matrix, made up of real elements whose identification is fast and immediate, depending on the type of constraints and on the cylinder geometrical and material properties. The high usability of this tool makes it suitable to be implemented without requiring any specific knowledge of the topic, fostering its adoption over a wide range of engineering fields. Moreover, it could be exploited for any combination of boundary conditions. Still, only simply supported and clamped ends are considered in this work, being the ones with the higher practical interest since the natural frequencies of any cylinder under an arbitrary degree of fixing, such as through flanges or end-plates, lie between the corresponding natural frequencies occurring with simply supported and clamped ends [14].

Section 2 outlines the equations of motion underpinning the new mathematical treatment to study the free vibrations problem for thin-walled cylinders. The proposed novel formulation to predict the natural frequencies is described in Section 3. Section 4 tests the model accuracy and its validity range by several comparisons with results obtained by the finite element method or available in the literature. Section 5 concludes this paper.

2. Equations of Motion for Thin Circular Cylindrical Shells

Consider an isotropic and homogeneous thin circular cylindrical shell with length l, uniform thickness h, mean radius r, Young's modulus E, Poisson's ratio ν, and density ρ. Figure 1 shows the coordinate system defined for the middle surface by the axial direction

x, the circumferential direction s, and the radial direction z. θ is the angular circumferential coordinate.

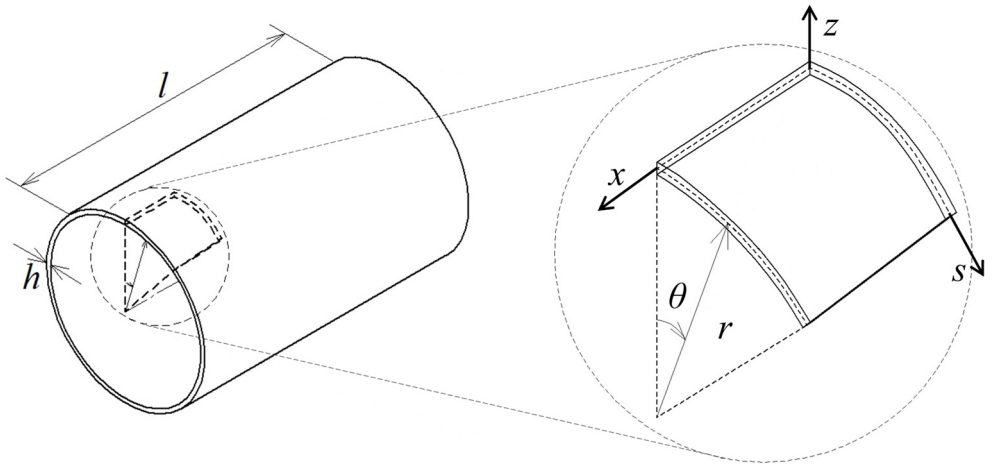

Figure 1. Geometry and coordinate system on the mid-surface for a thin-walled cylinder.

Considering a differential element of the cylindrical shell, the positive forces and moments acting per unit length are shown in Figure 2. For the face with normal along the x direction, N_x and N_{xs} are the in-plane normal and shear forces, Q_x is the out-of-plane shear force, and M_x and M_{xs} are the bending moment and torsional moment. The same considerations are valid, respectively, for N_s, N_{sx}, Q_s, M_{sx}, and M_s for the face with normal along the s direction.

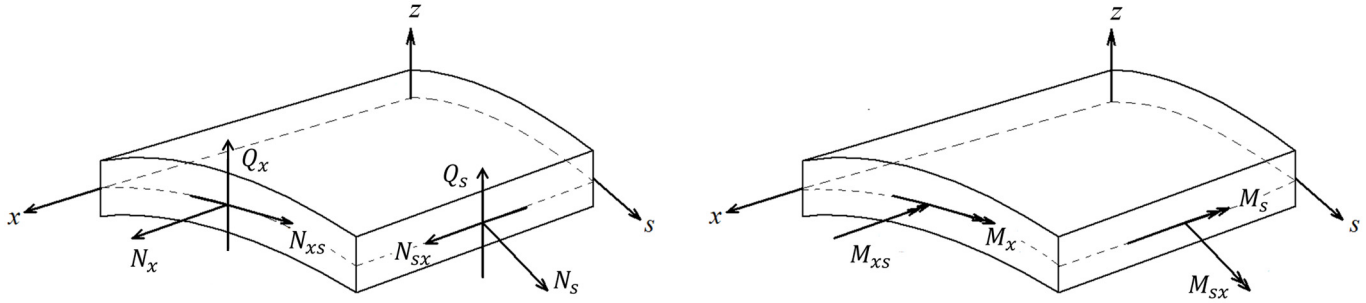

Figure 2. Positive forces and moments acting on a differential element.

The cylindrical shell theory adopted in the present research and outlined in this section is the Donnell–Mushtari version of Love's theory.

The resulting equations of motion derived from the translational equilibrium along x, s, and z are as follows:

$$\begin{aligned} \frac{\partial N_x}{\partial x} + \frac{\partial N_{sx}}{\partial s} &= \rho h \frac{d^2 u_x}{dt^2} \\ \frac{\partial N_s}{\partial s} + \frac{\partial N_{xs}}{\partial x} &= \rho h \frac{d^2 u_s}{dt^2} \\ \frac{\partial Q_s}{\partial s} + \frac{\partial Q_x}{\partial x} - \frac{N_s}{r} &= \rho h \frac{d^2 u_z}{dt^2} \end{aligned} \tag{1}$$

From the rotational equilibrium with respect to x and s, the relations between the transverse shear force resultants and the moment resultants reduce to:

$$\begin{aligned} \frac{\partial M_s}{\partial s} + \frac{\partial M_{xs}}{\partial x} - Q_s &= 0 \\ \frac{\partial M_x}{\partial x} + \frac{\partial M_{sx}}{\partial s} - Q_x &= 0 \end{aligned} \tag{2}$$

By substituting Equation (2) into the last of Equation (1), the latter reduces to:

$$\frac{\partial^2 M_x}{\partial x^2} + 2\frac{\partial^2 M_{xs}}{\partial x \partial s} + \frac{\partial^2 M_s}{\partial s^2} - \frac{N_s}{r} = \rho h \frac{d^2 u_z}{dt^2} \tag{3}$$

The strain–displacement relations are:

$$\begin{aligned} \varepsilon_x &= \frac{\partial u_x}{\partial x} \\ \varepsilon_s &= \frac{\partial u_s}{\partial s} + \frac{u_z}{r} \\ \gamma_{xs} &= \frac{\partial u_s}{\partial x} + \frac{\partial u_x}{\partial s} \\ k_x &= -\frac{\partial^2 u_z}{\partial x^2} \\ k_s &= \frac{\partial^2 u_z}{\partial s^2} \\ \tau &= -2\frac{\partial^2 u_z}{\partial x \partial s} \end{aligned} \tag{4}$$

where u_x, u_s, and u_z are the displacement components of a point on the middle surface along the axial, circumferential, and radial directions; ε_x and ε_s are the normal strains along x and s directions; γ_{xs} is the in-plane shear strain; k_x and k_s are the changes in the curvature of the mid-surface; and τ is the mid-surface twist. Note that $\varepsilon_r = \gamma_{sr} = \gamma_{xr} = 0$ for Love's hypotheses.

Lastly, the resultants of forces and moments are related to the stresses, which in turn are related to the strains by Hooke's law. Hence, the resulting forces and moments are reduced to the following functions of strains:

$$\begin{aligned} N_x &= K(\varepsilon_x + \nu\varepsilon_s) \\ N_s &= K(\varepsilon_s + \nu\varepsilon_x) \\ N_{xs} = N_{sx} &= \frac{K(1-\nu)}{2}\gamma_{xs} \\ M_x &= D(k_x + \nu k_s) \\ M_s &= D(k_s + \nu k_x) \\ M_{xs} = M_{sx} &= \frac{K(1-\nu)}{2}\tau \end{aligned} \tag{5}$$

where $K = \frac{Eh}{1-\nu^2}$ and $D = \frac{Eh^3}{12(1-\nu^2)}$ are, respectively, the tensile and bending stiffness of the cylindrical shell.

After substituting the strain–displacement relation of Equation (4) into Equation (5) and then introducing the latter into the first two equations of motion of Equation (1) and in Equation (3), considering that $ds = r{\cdot}d\theta$, the final equations of motion expressed as functions of displacements are:

$$\begin{aligned} K\left(\frac{\partial^2 u_x}{\partial x^2} + \frac{1-\nu}{2r^2}\frac{\partial^2 u_x}{\partial \theta^2} + \frac{1+\nu}{2r}\frac{\partial^2 u_s}{\partial x \partial \theta} + \frac{\nu}{r}\frac{\partial u_z}{\partial x}\right) &= \rho h \frac{d^2 u_x}{dt^2} \\ K\left(\frac{1}{r^2}\frac{\partial^2 u_s}{\partial \theta^2} + \frac{1-\nu}{2}\frac{\partial^2 u_s}{\partial x^2} + \frac{1+\nu}{2r}\frac{\partial^2 u_x}{\partial x \partial \theta} + \frac{1}{r^2}\frac{\partial u_z}{\partial \theta}\right) &= \rho h \frac{d^2 u_s}{dt^2} \\ K\left[-\frac{\nu}{r}\frac{\partial u_x}{\partial x} - \frac{1}{r^2}\frac{\partial u_s}{\partial \theta} - \frac{u_z}{r^2} - \frac{h^2}{12}\left(\frac{\partial^4 u_z}{\partial x^4} + \frac{1}{r^4}\frac{\partial^4 u_z}{\partial \theta^4} + \frac{2}{r^2}\frac{\partial^4 u_z}{\partial x^2 \partial \theta^2}\right)\right] &= \rho h \frac{d^2 u_z}{dt^2} \end{aligned} \tag{6}$$

Equation (6) constitute an eighth-order system of coupled partial differential equations in terms of the three displacement components. Under the hypothesis of a small thickness, the dependence of the three displacement components from the radial coordinate can be neglected; thus, the general expression of the eigenfunctions of the problem is:

$$\begin{cases} u_x = F_x(x, \theta, t) \\ u_s = F_s(x, \theta, t) \\ u_z = F_z(x, \theta, t) \end{cases} \tag{7}$$

where t is the time coordinate. Four boundary conditions for each cylinder end must be introduced to solve the problem. Nevertheless, an exact solution is not available in an explicit form for any combination of boundary constraints. Thus, an approximated resolution based on an energetic method is described in the next section.

3. Generalised Eigenvalue Problem for Natural Frequencies

The most common methods to simplify the free vibrations problem of thin-walled cylinders are based on energetic variational approaches similarly to the Rayleigh–Ritz method. The system of partial differential equations derived from the fundamental theories of thin cylindrical shells (Equation (6)) is reduced to a simpler system of ordinary differential equations by assuming reasonable eigenfunctions for the three displacement components so as not to violate the end conditions, and introducing the equations of motion and the assumed eigenfunctions in an energetic principle. Hence, the resulting solution is not exact but approximately correct on the whole domain.

From the experimental evidence, each vibrational mode of a cylindrical shell is characterised by the number of transverse half-waves, denoted by the positive integer m, and the number of circumferential waves, indicated by the positive integer n. The relevant literature reports several applications proving that fairly accurate results are achieved if a particular solution for a given mode, identified by specific m and n values, is derived by performing a variables separation in the displacements eigenfunctions while ensuring the compliance with the end conditions and the periodicity of the circumferential waveform. Thus, the three coordinates x, θ, and t can be decoupled as follows:

$$\begin{cases} u_x(x,\theta,t) = A_x \frac{d\mathcal{F}_m(X)}{dX} \cos n\theta \cos \omega t \\ u_s(x,\theta,t) = A_s \mathcal{F}_m(X) \sin n\theta \cos \omega t \\ u_z(x,\theta,t) = A_z \mathcal{F}_m(X) \cos n\theta \cos \omega t \end{cases} \tag{8}$$

where $X = x/l$ is the axial coordinate normalised to the cylinder length; A_x, A_s, and A_z are constant displacement amplitudes; and $\mathcal{F}_m(X)$ is the mth transverse waveform of a beam constrained as the cylinder under analysis, which can be generalised as:

$$\mathcal{F}_m(X) = C_1 \cos \beta_m X + C_2 \cosh \beta_m X + C_3 \sin \beta_m X + C_4 \sinh \beta_m X \tag{9}$$

where C_1, C_2, C_3, and C_4 are constant values depending on m and the boundary constraints. For a simply supported end, the latter result in the following conditions is:

$$u_s = u_z = N_x = M_x = 0 \tag{10}$$

For a clamped end, it is:

$$u_x = u_s = u_z = \frac{\partial u_z}{\partial x} = 0 \tag{11}$$

Table 1 lists the flexural waveforms and the frequency equations for a beam subject to the boundary conditions of interest, which are well-established in the relevant literature [20]. For given constraints, each mth waveform of the beam depends on the mth root of the transcendental frequency equation, denoted by β_m. Note that the transverse waveform is the same for both ends clamped or one clamped and one simply supported, but the frequency equation and the related solutions differ.

At this point, the equations of motion of Equation (6) are introduced in the principle of virtual work, according to which the virtual work δW of all the forces acting on the system, including the inertial actions, is null for any virtual displacements δu_x, δu_s, and δu_z that do not violate the boundary conditions:

$$\begin{aligned} \delta W = rK \int_0^{2\pi} \int_0^l \Bigg\{ & \left[\frac{\partial^2 u_x}{\partial x^2} + \frac{1-v}{2r^2} \frac{\partial^2 u_x}{\partial \theta^2} + \frac{1+v}{2r} \frac{\partial^2 u_s}{\partial x \partial \theta} + \frac{v}{r} \frac{\partial u_z}{\partial x} - \frac{1-v^2}{E} \rho \frac{d^2 u_x}{dt^2} \right] \delta u_x \\ & + \left[\frac{1}{r^2} \frac{\partial^2 u_s}{\partial \theta^2} + \frac{1-v}{2} \frac{\partial^2 u_s}{\partial x^2} + \frac{1+v}{2r} \frac{\partial^2 u_x}{\partial x \partial \theta} + \frac{1}{r^2} \frac{\partial u_z}{\partial \theta} - \frac{1-v^2}{E} \rho \frac{d^2 u_s}{dt^2} \right] \delta u_s \\ & - \left[\frac{v}{r} \frac{\partial u_x}{\partial x} + \frac{1}{r^2} \frac{\partial u_s}{\partial \theta} + \frac{u_z}{r^2} + \frac{h^2}{12} \left(\frac{\partial^4 u_z}{\partial x^4} + \frac{1}{r^4} \frac{\partial^4 u_z}{\partial \theta^4} + \frac{2}{r^2} \frac{\partial^4 u_z}{\partial x^2 \partial \theta^2} \right) + \frac{1-v^2}{E} \rho \frac{d^2 u_z}{dt^2} \right] \delta u_z \Bigg\} dx d\theta = 0 \end{aligned} \tag{12}$$

Table 1. Flexural waveforms of a beam as a function of the normalised axial coordinate $X = x/l$ for different constraints. C_m is an arbitrary amplitude constant.

Boundary Conditions	Frequency Equation	Roots of Frequency Equation	Flexural Waveform
Simply supp./Simply supp.	$\sin\beta_m = 0$	$\beta_m = m\pi$ for $m = 1, 2, 3, \ldots$	$\mathcal{F}_m(X) = C_m \sin\beta_m X$
Clamped/Clamped	$\cos\beta_m \cosh\beta_m = 1$	$\beta_1 = 4.73004$ $\beta_2 = 7.85320$ $\beta_m = (2m+1)\frac{\pi}{2}$ for $m \geq 3$	$\mathcal{F}_m(X) =$ $C_m[(\cos\beta_m X - \cosh\beta_m X) -$ $\frac{\cos\beta_m - \cosh\beta_m}{\sin\beta_m - \sinh\beta_m}(\sin\beta_m X - \sinh\beta_m X)]$
Clamped/Simply supported	$\tan\beta_m - \tanh\beta_m = 0$	$\beta_1 = 3.92660$ $\beta_2 = 7.06858$ $\beta_m = (4m+1)\frac{\pi}{4}$ for $m \geq 3$	$\mathcal{F}_m(X) =$ $C_m[(\cos\beta_m X - \cosh\beta_m X) -$ $\frac{\cos\beta_m - \cosh\beta_m}{\sin\beta_m - \sinh\beta_m}(\sin\beta_m X - \sinh\beta_m X)]$

Given the arbitrariness of the virtual displacements δu_x, δu_s, and δu_z, Equation (12) can be satisfied if each of the three addends is null. Thus, the problem is reduced to the following three-equation system, obtained by normalising to the cylinder length l:

$$\begin{cases} \int_0^{2\pi}\int_0^1 \left[\left(\frac{\partial^2 u_x}{\partial X^2} + \frac{1-\nu}{2R^2}\frac{\partial^2 u_x}{\partial^2} + \frac{1+\nu}{2R}\frac{\partial^2 u_s}{\partial X \partial\theta} + \frac{\nu}{R}\frac{\partial u_z}{\partial X} - \frac{1-\nu^2}{E}\rho l^2 \frac{d^2 u_x}{dt^2}\right)\delta u_x\right] dX d\theta = 0 \\ \int_0^{2\pi}\int_0^1 \left[\left(\frac{1}{R^2}\frac{\partial^2 u_s}{\partial\theta^2} + \frac{1-\nu}{2}\frac{\partial^2 u_s}{\partial X^2} + \frac{1+\nu}{2R}\frac{\partial^2 u_x}{\partial X \partial\theta} + \frac{1}{R^2}\frac{\partial u_z}{\partial\theta} - \frac{1-\nu^2}{E}\rho l^2 \frac{d^2 u_s}{dt^2}\right)\delta u_s\right] dX d\theta = 0 \\ \int_0^{2\pi}\int_0^1 \left\{\left[\frac{\nu}{R}\frac{\partial u_x}{\partial X} + \frac{1}{R^2}\frac{\partial u_s}{\partial\theta} + \frac{u_z}{R^2} + \frac{H^2}{12}\left(\frac{\partial^4 u_z}{\partial X^4} + \frac{1}{R^4}\frac{\partial^4 u_z}{\partial\theta^4} + \frac{2}{R^2}\frac{\partial^4 u_z}{\partial X^2 \partial\theta^2}\right) + \frac{1-\nu^2}{E}\rho l^2 \frac{d^2 u_z}{dt^2}\right]\delta u_z\right\} dX d\theta = 0 \end{cases} \quad (13)$$

where $R = r/l$ is the cylinder mean radius normalised to the length and $H = h/l$ is the normalised thickness.

The system of Equation (13) can be reduced by introducing the assumed eigenfunctions of Equation (8) for the displacement components and their partial derivatives. In particular, consider that for each displacement component $\frac{d^2 u_i}{dt^2} = -\omega^2 u_i$ and $\delta u_i = \delta A_i u_i / A_i$ where δA_i is arbitrary, the reduced system does not depend on the time coordinate t; indeed, each term of the equations would be multiplied by $\cos^2 \omega t$, which is constant within the integration domain and thus can be simplified. Moreover, the dependence on the circumferential coordinate θ can also be eliminated, because it reduces to $\int_0^{2\pi} \cos^2 n\theta d\theta = \pi$ for the first and the third equation and to $\int_0^{2\pi} \sin^2 n\theta d\theta = \pi$ for the second one. Hence, after some mathematical manipulation, Equation (13) is reduced to the following homogeneous linear system:

$$\begin{cases} I_{13}A_x - \frac{1-\nu}{2R^2}n^2 I_{11}A_x + \frac{1+\nu}{2R}n I_{11}A_s + \frac{\nu}{R}I_{11}A_z + \Delta\, I_{11}A_x = 0 \\ \frac{-n^2}{R^2}I_{00}A_s + \frac{1-\nu}{2}I_{02}A_s - \frac{1+\nu}{2R}n I_{02}A_x - \frac{n}{R^2}I_{00}A_z + \Delta\, I_{00}A_s = 0 \\ \frac{\nu}{R}I_{02}A_x + \frac{n}{R^2}I_{00}A_s + \frac{1}{R^2}I_{00}A_z + \frac{H^2}{12}\left(I_{04}A_z + \frac{n^4}{R^4}I_{00}A_z - \frac{2n^2}{R^2}I_{02}A_z\right) - \Delta\, I_{00}A_z = 0 \end{cases} \quad (14)$$

where $\Delta = \frac{1-\nu^2}{E}\rho l^2 \omega^2$. The notation I_{ij} is the definite integral from 0 to 1 of the product between the ith- and jth-order derivatives of the function $\mathcal{F}_m(X)$ for a given number m of flexural half-waves:

$$I_{ij} = \int_0^1 \frac{d^i}{dX^i}\mathcal{F}_m(X) \cdot \frac{d^j}{dX^j}\mathcal{F}_m(X) dX \quad \text{for } i = 0, 1 \text{ and } j = 0, 1, 2, 3, 4 \quad (15)$$

The zero-order derivative is the function $\mathcal{F}_m(X)$ itself.

After simple mathematical manipulation, Equation (14) reduces to the following matrix formulation:

$$\left(\overline{\overline{D}} - \Delta\,\overline{\overline{I}}\right)\{A\} = \{0\} \quad (16)$$

where $\{A\} = \{A_x; A_s; A_z\}$ is the unknown vector containing the displacements amplitudes in the three directions, $\overline{\overline{I}}$ is the identity matrix, and $\overline{\overline{D}}$ is the following matrix:

$$\overline{\overline{D}} = \begin{bmatrix} -\frac{I_{13}}{I_{11}} + \frac{1-\nu}{2R^2}n^2 & -n\frac{1+\nu}{2R} & -\frac{\nu}{R} \\ \frac{1+\nu}{2}\frac{n}{R}\frac{I_{02}}{I_{00}} & -\frac{1-\nu}{2}\frac{I_{02}}{I_{00}} + \frac{n^2}{R^2} & \frac{n}{R^2} \\ \frac{\nu}{R}\frac{I_{02}}{I_{00}} & \frac{n}{R^2} & \frac{1}{R^2} + \frac{H^2}{12}\left(\frac{I_{04}}{I_{00}} + \frac{n^4}{R^4} - \frac{2}{R^2}n^2\frac{I_{02}}{I_{00}}\right) \end{bmatrix} \quad (17)$$

As it is apparent from Equation (16), the natural frequency of any thin-walled cylinder can be easily calculated by solving the eigenvalue problem of the matrix $\overline{\overline{D}}$, which, thus, is equivalent to a typical dynamic matrix in the modal analysis of discreet systems. From the three eigenvalues Δ_1, Δ_2, and Δ_3, the natural frequency is obtained as follows:

$$f_i = \frac{1}{2\pi}\sqrt{\frac{E\Delta_i}{(1-\nu^2)\rho l^2}} \quad for\ i = 1,\ 2,\ 3 \quad (18)$$

The eigenvectors corresponding to each eigenvalue determine the ratios between the amplitude of the axial, circumferential, and radial displacements for any mode shape.

It is crucial to notice that the integrals of Equation (15) are univocally defined only by the specific m and the cylinder boundary conditions because of the normalisation to the cylinder length. Moreover, from Equations (9) and (15), it can be easily derived that:

$$\frac{I_{04}}{I_{00}} = \beta_m^4 \quad (19)$$

where β_m can be derived from Table 1. Hence, only the following ratios must be calculated:

$$\begin{aligned} \frac{I_{13}}{I_{11}} &= \frac{\int_0^1 \frac{d\mathcal{F}_m(X)}{dX}\cdot\frac{d^3\mathcal{F}_m(X)}{dX^3}dX}{\int_0^1\left(\frac{d\mathcal{F}_m(X)}{dX}\right)^2 dX} \\ \frac{I_{02}}{I_{00}} &= \frac{\int_0^1 \mathcal{F}_m(X)\cdot\frac{d^2\mathcal{F}_m(X)}{dX^2}dX}{\int_0^1 \mathcal{F}_m^2(X)dX} \end{aligned} \quad (20)$$

Tables 2–4 list the values of interest of Equation (20), which are derived from the beam flexural waveforms of Table 1 for the corresponding end condition and can be used in Equation (17) for any thin cylindrical shell.

Table 2. Numerical values for integrals ratios for any cylinder with two simply supported ends for $m \leq 8$.

	$m = 1$	$m = 2$	$m = 3$	$m = 4$	$m = 5$	$m = 6$	$m = 7$	$m = 8$
$\frac{I_{13}}{I_{11}}$	−9.870	−39.478	−88.826	−157.914	−246.740	−355.306	−483.611	−631.655
$\frac{I_{02}}{I_{00}}$	−9.870	−39.478	−88.826	−157.914	−246.740	−355.306	−483.611	−631.655

Table 3. Numerical values for integrals ratios for any cylinder with two clamped ends for $m \leq 8$.

	$m = 1$	$m = 2$	$m = 3$	$m = 4$	$m = 5$	$m = 6$	$m = 7$	$m = 8$
$\frac{I_{13}}{I_{11}}$	−40.688	−82.596	−147.795	−232.792	−337.637	−462.266	−606.660	−770.810
$\frac{I_{02}}{I_{00}}$	−12.303	−46.050	−98.905	−171.586	−263.998	−376.150	−508.041	−659.673

As a result, populating the dynamic matrix $\overline{\overline{D}}$ and solving its eigenvalue problem is immediate and straightforward once the cylinder geometry (R, H, l), the material properties (ν, E, ρ), the vibrational mode (m, n), and the end constraints (Tables 2–4) are known.

Table 4. Numerical values for integrals ratios for any clamped/simply supported cylinder for $m \leq 8$.

	$m = 1$	$m = 2$	$m = 3$	$m = 4$	$m = 5$	$m = 6$	$m = 7$	$m = 8$
$\frac{I_{13}}{I_{11}}$	−20.649	−58.198	−115.566	−192.702	−289.589	−406.220	−542.594	−698.708
$\frac{I_{02}}{I_{00}}$	−11.513	−42.896	−94.038	−164.918	−255.538	−365.896	−495.995	−645.832

4. Results and Discussion

The procedure described in Section 3 was carried out for cylinders with different geometry and material under the three end conditions of interest, i.e., two simply supported ends, two clamped ends, and one clamped and one simply supported end. The eigenvalue problem for the dynamic matrix $\overline{\overline{D}}$ was performed in MATLAB R2022a numerical software.

Firstly, the natural frequencies and the displacement amplitudes' ratios of a steel cylinder ($\rho = 7833\ \mathrm{kg/m^3}$, $E = 207\ \mathrm{kN/mm^2}$, $\nu = 0.3$) with mean radius $r = 76$ mm, length $l = 305$ mm, and thickness $h = 0.254$ mm were assessed in the three scenarios. The trend of the resulting natural frequencies agrees with the vibrational behaviour of thin-walled cylinders predicted by the relevant literature [11,15–17,29,33,35,46,50,52,54,56]; therefore, the results of this first analysis, discussed in Section 4.1, are listed in the Appendix A. On the contrary, the numerical and graphical results presented in the current section focus on the model validation.

The same steel cylinder defined above was considered to test the model accuracy by assuming the results of an FEM analysis as a benchmark, as addressed in Section 4.2. Section 4.3 proposes a sensitivity analysis of the present model with respect to cylinder geometry and material, presenting a validity range whereby the maximum error against FEM is approximately 10%. Lastly, Section 4.4 compares the present model with the results obtained by some experimental, numerical, and analytical methods available in the literature.

For Sections 4.1–4.3, all the mode shapes with $m \leq 8$ and $n \leq 14$ were examined. Nonetheless, the natural frequencies for $m > 4$ are not listed in the Appendix A and in Section 4.2 for brevity, but the general considerations made in Sections 4.1 and 4.2 remain valid also for $m \geq 4$. Moreover, as it is common in the literature on the topic, only the first natural frequency is considered for the model validation carried out in Sections 4.2–4.4, being the lowest natural frequency as it is addressed in Section 4.1, and thus the one to be monitored to prevent the undesired risk of resonance phenomena.

4.1. Natural Frequencies and Amplitude Ratios

Tables A1–A3 list the results for the natural frequencies associated with each mode shape (m, n) for every boundary condition derived from the eigenvalues of the dynamic matrix. It is apparent that the first frequency f_1 is lower than f_2 and f_3 by up to two orders of magnitude. Moreover, it is worth noting that f_2 and f_3 are monotonically increasing for increasing m and n, while f_1 shows a minimum for a number n of circumferential waves that increases with the considered number m of transverse half-waves. In Tables A1–A3, the minimum value of f_1 for a given number m of transverse half-waves is underlined. This general trend for the frequency f_1 was explained by Arnold and Warburton in [11] by the opposite variation of the stretching energy, which decreases with the number of circumferential waves, and the bending energy, which, on the contrary, increases; as a result, the minimum of the lowest natural frequency f_1 for a given number m of transverse half-waves is due to a minimum in the total strain energy. Nonetheless, depending on the cylinder geometry, f_1 can show a monotonic trend for a low number of transverse half-waves. The global minimum of f_1, highlighted in bold in Tables A1–A3, occurs for $m = 1$ and $n = 5$ if the cylinder has one or two simply supported ends; instead, it occurs for $m = 1$ and $n = 6$ for the clamped/clamped cylinder. Furthermore, for each mode shape (m,n), the natural frequencies of the clamped/simply supported cylinder (Table A3) are intermediate between those of the simply supported/simply supported cylinder (Table A1),

which are the lowest, and clamped/clamped cylinder (Table A2), which are the highest. This evidence validates the hypothesis that the natural frequencies of any cylinder under an arbitrary degree of fixing lie between the natural frequencies achieved for simply supported and clamped ends [14], corroborating the generality of this work.

Tables A4–A6 show the amplitude ratios derived from the eigenvectors of each mode shape only for $n \leq 7$, for brevity. The amplitude of the radial displacement A_z is chosen as the normalising term. The predominant motion associated with the frequency f_1 is the radial one, while the circumferential displacement and, above all, the axial displacement are small. Thus, the first frequency implies a transverse vibrational mode, whose displacement amplitude increases for increasing m and n. On the contrary, for f_2 and f_3, the amplitude of the radial displacement decreases for increasing m and n. Nonetheless, for the second frequency f_2, A_x grows faster than A_s for $m = 1$; thus, an axial motion is predominant for any n for a simply supported/simply supported cylinder, $n \geq 4$ for a clamped/clamped cylinder, and $n \geq 3$ for a clamped/simply supported cylinder. For $m \geq 2$, f_2 mainly involves a predominant circumferential motion. The third frequency f_3 is always associated with a predominant circumferential motion. Similar trends were obtained in [46] for the amplitude ratios of a clamped/clamped cylinder.

4.2. Comparison with FEM Results

To test the accuracy of the novel approximated method, the results of a simulations campaign carried out in the commercial software Ansys 22.1, based on the finite element method, were considered as a benchmark. For this purpose, SHELL181 linear elements were used for the modal analysis. Tables 5–7 compare the first frequency f_1 obtained by the approximated method and the FEM analysis, reporting the percentage error between the two approaches. Overall, for the cylinder with two simply supported ends, the error is far lower than $\pm 1\%$ and mainly negative, which means that the first natural frequency is slightly underestimated on average. On the contrary, the error is higher and mainly positive for the other two end conditions. In Tables 5–7, the error related to the global minimum of f_1 is underlined in bold, while an asterisk indicates the maximum error. In this regard, the maximum error between the fast approximated method and the FEM for the simply supported/simply supported cylinder is 2.07% and occurs for $m = 1$ and $n = 6$; instead, the maximum error is 9.82% and 11.9% for the clamped/clamped or clamped/simply supported cylinder, respectively; in both cases, it occurs for $m = n = 1$. Nonetheless, the error occurring for the global minimum frequency, the most potentially dangerous, is just 2.01%, 3.05%, and 3.66%, respectively. Therefore, the level of accuracy is satisfactory.

Table 5. First natural frequency f_1 assessed by the present model and FEM modal analysis and percentage error. Results for a steel cylinder with two simply supported ends for $m \leq 4$ and $n \leq 14$. The error for the global minimum is underlined in bold; an asterisk indicates the maximum error.

n	$m = 1$			$m = 2$			$m = 3$			$m = 4$		
	f_1(Hz)		Error (%)	f_1(Hz)		Error (%)	f_1(Hz)		Error (%)	f_1(Hz)		Error (%)
	Present	FEM		Present	FEM		Present	FEM		Present	FEM	
1	2885.89	2885.9	−0.0004	6444.7	6445.3	−0.010	8555.7	8557.3	−0.018	9527.5	9529.5	−0.021
2	1265.13	1265.0	0.011	3676.6	3677.5	−0.025	5820.8	5823.2	−0.043	7344.4	7348.5	−0.055
3	656.0	654.8	0.19	2178.1	2178.8	−0.034	3896.1	3898.9	−0.071	5413.0	5418.2	−0.096
4	422.7	418.7	0.96	1396.4	1396.3	0.0093	2681.1	2683.5	−0.092	3986.1	3991.5	−0.14
5	372.0	364.7	**2.01**	985.3	983.5	0.18	1931.4	1933.0	−0.082	2994.2	2999.2	−0.17
6	431.4	422.6	2.07 *	792.1	788.1	0.51	1477.2	1477.4	−0.013	2322.6	2326.7	−0.18
7	550.6	542.2	1.56	751.4	745.7	0.76	1226.6	1225.2	0.12	1884.4	1887.3	−0.15
8	705.3	698.2	1.02	818.6	812.7	0.72	1131.6	1129.0	0.23	1626.4	1628.0	−0.10
9	886.7	881.8	0.56	955.9	951.5	0.47	1157.8	1155.3	0.21	1515.7	1516.8	−0.072
10	1091.9	1090.1	0.17	1138.9	1137.3	0.15	1272.5	1271.8	0.048	1525.7	1527.6	−0.12
11	1319.7	1322.2	−0.18	1355.2	1357.7	−0.18	1448.9	1451.8	−0.20	1629.6	1634.1	−0.28
12	1569.7	1577.7	−0.51	1599.0	1607.0	−0.50	1669.5	1677.7	−0.49	1803.0	1812.1	−0.50

Table 5. *Cont.*

n	$m = 1$			$m = 2$			$m = 3$			$m = 4$		
	f_1(Hz)		Error (%)	f_1(Hz)		Error (%)	f_1(Hz)		Error (%)	f_1(Hz)		Error (%)
	Present	FEM		Present	FEM		Present	FEM		Present	FEM	
13	1841.6	1856.9	−0.82	1867.4	1882.6	−0.81	1924.4	1939.5	−0.78	2027.9	2043.6	−0.77
14	2135.5	2159.9	−1.13	2159.2	2183.5	−1.11	2207.9	2232.1	−1.09	2292.5	2316.9	−1.05

Table 6. First natural frequency f_1 assessed by the present model and FEM modal analysis and percentage error. Results for a steel cylinder with two clamped ends for $m \leq 4$ and $n \leq 14$. The error for the global minimum is underlined in bold; an asterisk indicates the maximum error.

n	$m = 1$			$m = 2$			$m = 3$			$m = 4$		
	f_1(Hz)		Error (%)	f_1(Hz)		Error (%)	f_1(Hz)		Error (%)	f_1(Hz)		Error (%)
	Present	FEM		Present	FEM		Present	FEM		Present	FEM	
1	3788	3450	9.82 *	6933	6524	6.27	8781	8759	0.25	9670	9644	0.28
2	2084	1996	4.40	4320	3945	9.50	6192	5975	3.62	7555	7530	0.32
3	1233	1185	4.09	2793	2555	9.30	4360	4109	6.10	5723	5578	2.59
4	806	769	4.79	1901	1852	2.67	3142	2947	6.63	4348	4173	4.20
5	605	581	4.11	1375	1311	4.84	2342	2208	6.07	3360	3202	4.91
6	555	538	**3.05**	1077	1036	3.94	1821	1809	0.69	2661	2543	4.65
7	611	600	1.88	943	916	2.92	1500	1465	2.39	2181	2096	4.04
8	736	729	0.97	938	921	1.75	1335	1311	1.83	1873	1930	−2.94
9	903	897	0.71	1027	1015	1.26	1300	1276	1.94	1711	1669	2.49
10	1102	1099	0.25	1183	1176	0.57	1369	1354	1.10	1672	1646	1.61
11	1326	1328	−0.13	1383	1382	0.071	1513	1507	0.42	1736	1721	0.84
12	1574	1582	−0.46	1618	1623	−0.33	1714	1715	−0.11	1879	1875	0.21
13	1845	1860	−0.78	1881	1894	−0.68	1956	1966	−0.53	2083	2090	−0.30
14	2138	2162	−1.09	2170	2192	−1.01	2231	2251	−0.90	2334	2351	−0.73

Table 7. First natural frequency f_1 assessed by the present model and FEM modal analysis and percentage error. Results for a steel clamped/simply supported cylinder for $m \leq 4$ and $n \leq 14$. The error for the global minimum is underlined in bold; an asterisk indicates the maximum error.

n	$m = 1$			$m = 2$			$m = 3$			$m = 4$		
	f_1(Hz)		Error (%)	f_1(Hz)		Error (%)	f_1(Hz)		Error (%)	f_1(Hz)		Error (%)
	Present	FEM		Present	FEM		Present	FEM		Present	FEM	
1	3485	3115	11.88 *	6720	6449	4.21	8676	8558	1.38	9603	9532	0.75
2	1737	1602	8.40	4040	3813	5.97	6026	5851	2.98	7457	7353	1.42
3	957	904	5.87	2512	2378	5.63	4149	3991	3.96	5580	5451	2.36
4	609	583	4.52	1661	1588	4.60	2928	2816	3.96	4180	4063	2.87
5	476	460	**3.66**	1183	1141	3.66	2146	2074	3.49	3187	3097	2.89
6	482	469	2.72	932	906	2.88	1653	1607	2.89	2499	2435	2.62
7	574	564	1.82	842	825	2.13	1364	1333	2.29	2037	1992	2.22
8	717	709	1.14	873	861	1.41	1232	1212	1.68	1751	1721	1.75
9	893	888	0.62	988	980	0.81	1226	1213	1.08	1613	1665	−3.13
10	1096	1094	0.21	1158	1155	0.33	1318	1311	0.54	1598	1593	0.29
11	1322	1324	−0.15	1368	1369	−0.073	1479	1478	0.08	1681	1677	0.26
12	1572	1579	−0.48	1607	1614	−0.42	1690	1695	−0.31	1840	1843	−0.16
13	1843	1858	−0.79	1874	1888	−0.75	1939	1952	−0.67	2054	2066	−0.55
14	2137	2161	−1.10	2164	2187	−1.06	2219	2241	−1.00	2312	2333	−0.90

Figure 3 graphically summarises the results of the comparison with the FEM analysis, showing the trend of f_1 for $m \leq 8$ and $n \leq 14$. The minimum value of f_1 for each m is indicated by a black dot.

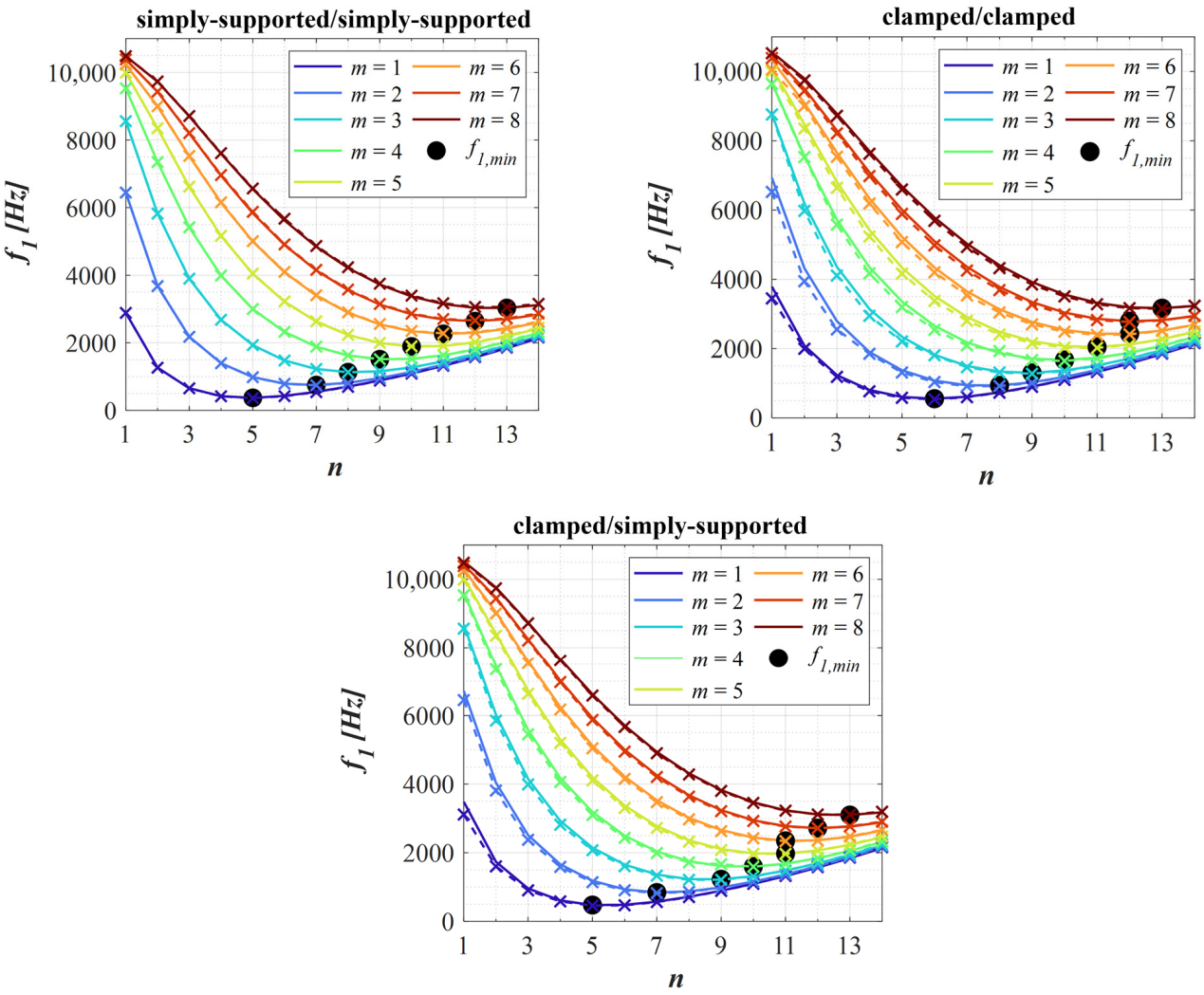

Figure 3. Comparison between the novel model and FEM analysis for any boundary condition. The present results are represented by continuous lines; FEM results are represented by X markers and dotted lines; a black dot indicates the minimum frequency for a given m.

4.3. Influence of Cylinder Geometry and Material on Model Accuracy

To further explore the potentiality of the model, its accuracy was tested for different cylinder geometry and material within $m \leq 8$ and $n \leq 14$. Starting from the reference steel cylinder with $l/r = 4$ and $h/r = 1/300$, cylinder length and thickness were changed in turn to assess how they affect model performance for any boundary condition. The observed ranges of variation are $2 \leq l/r \leq 10$ and $1/400 \leq h/r \leq 1/20$. For this purpose, it was sufficient to accordingly change R or H in the dynamic matrix $\overline{\overline{D}}$ and repeat the resolution of the eigenvalue problem. FEM simulations were conducted to obtain the benchmark values for the first frequency f_1.

Table 8 lists the acceptable range of variation of l/r and h/r to comply with a maximum error of the model against the FEM results of approximately 10%. It also reports the maximum error for the global minimum frequency observed within the acceptable range. For any boundary conditions, the model accuracy increases for thinner cylinders. All other conditions being equal, the maximum acceptable value of the thickness/radius ratios is higher for the simply supported/simply supported cylinder, accordingly to the higher model accuracy observed for this boundary condition. On the contrary, the model accuracy improves for long cylinders with two clamped ends and for short cylinders with two simply supported ends. This trend affects the accuracy for a clamped/simply supported

cylinder, which shows an intermediate behaviour. Even though the acceptable ranges listed in Table 8 involve a maximum error of approximately 10%, the error related to the global minimum frequency is approximately 5% only.

Table 8. Results of the sensitivity analysis for a different cylinder length and thickness; the acceptable range provides an error within 10%.

Boundary Conditions	Influence of l/r		Influence of h/r	
	Acceptable Range	Error for Minimum f_1	Acceptable Range	Error for Minimum f_1
Simply supp./Simply supp.	$l/r \leq 10$	4.54%	$h/r \leq 1/20$	4.92%
Clamped/Clamped	$l/r \geq 3.3$	3.83%	$h/r \leq 1/100$	5.46%
Clamped/Simply supported	$l/r \leq 2.4$ and $l/r \geq 6$	4.58%	$h/r \leq 1/100$	5.28%

Table 9 compares the maximum error and the error for the lowest f_1 for a steel and an aluminium cylinder ($\rho = 2700$ kg/m^3, $E = 68.2$ kN/mm^2, $\nu = 0.33$) with $r = 76$ mm, $l = 305$ mm, and $h = 0.254$ mm. There are no significant differences, suggesting that the model performance is not affected by the cylinder material.

Table 9. Results of the sensitivity analysis for a different cylinder material.

Boundary Conditions	Steel		Aluminium	
	Maximum Error	Error for Minimum f_1	Maximum Error	Error for Minimum f_1
Simply supp./Simply supp.	2.07%	2.01%	2.07%	4.92%
Clamped/Clamped	9.82%	3.05%	9.82%	5.46%
Clamped/Simply supported	11.88%	3.66%	11.88%	5.28%

4.4. Comparison with the Literature

A further test on the validity of the proposed model is performed by considering data available in the literature. This section compares several experimental, numerical, and analytical methods of simply supported/simply supported and clamped/clamped thin-walled cylinders. Different cylinder geometry and material are considered. Experimental or FEM results are always assumed as the benchmark to assess the percentage difference. For brevity, when results for different numbers of transverse half-waves were available, the numerical values listed in the tables reported in the remainder of the section are generally those for $m = 1$, whereby the lowest frequencies are observed. The clamped/simply supported condition is not considered here due to the lack of FEM and experimental data in the literature. Table 10 summarises the literature comparison.

The natural frequencies of an aluminium simply supported/simply supported cylinder were experimentally assessed by Sewall and Naumann [15] in 1968. After that, the same cylinder was considered by Naeem and Sharma [50] to present a procedure based on the Rayleigh–Ritz variational approach. The transverse waveforms are modelled by Ritz polynomial functions, resulting in the formulation of an eigenvalue problem which is rather cumbersome, requiring analytical integrations and differentiations. The experimental results were available for $m = 1$ and $4 \leq n \leq 13$. Figure 4 shows the results of the comparison. From the numerical comparison reported in Table 11, the maximum percentage difference of the present model against the experimental data is 4.30% for $n = 13$, while Naeem and Sharma's model shows a maximum difference of -4.81% for $n = 6$. The error in the global minimum frequency for $n = 7$ is -0.36% for the present model and 1.64% for Naeem and Sharma. Other experimental results were formerly obtained by Arnold and Warburton [11] in 1949 for a steel simply supported/simply supported cylinder. Results were available for $m \leq 10$ and $2 \leq n \leq 6$. From Table 12, which reports the results of the comparison for $m \leq 4$ for brevity, the maximum percentage difference, observed for the global minimum frequency, is 16.22% for $m = 1$ and $n = 2$. Complete results are shown in Figure 5.

Table 10. Summary of the literature comparison.

Reference	Method	Boundary Conditions	Cylinder Material	Cylinder Geometry
Sewall and Naumann [15]	experimental	Simply supp./Simply supp.	aluminium: $\rho = 2715$ kg/m^3, $E = 69$ kN/mm^2, $\nu = 0.315$	$r = 242.3$ mm, $l = 609.6$ mm, $h = 0.648$ mm
Naeem and Sharma [50]	analytical			
Arnold and Warburton [11]	experimental	Simply supp./Simply supp.	steel: $\rho = 7833$ kg/m^3, $E = 207$ kN/mm^2, $\nu = 0.29$	$r = 48.9$ mm, $l = 397$ mm, $h = 2.5654$ mm
Pellicano [29]	numerical	Simply supp./Simply supp.	aluminium: $\rho = 2796$ kg/m^3, $E = 71$ kN/mm^2, $\nu = 0.31$	$r = 100$ mm, $l = 200$ mm, $h = 0.247$ mm
		Clamped/Clamped		
Xuebin [54]	analytical	Clamped/Clamped	aluminium: $\rho = 2700$ kg/m^3, $E = 64.7$ kN/mm^2, $\nu = 0.329$	$r = 153.5$ mm, $l = 800$ mm, $h = 1.1016$ mm
Koval and Cranch [16]	experimental	Clamped/Clamped	steel: $\rho = 7833$ kg/m^3, $E = 207$ kN/mm^2, $=0.3$	$r = 76$ mm, $l = 305$ mm, $h = 0.254$ mm
Xing et al. [33]	numerical			
Wang and Lai [53]	analytical			
Moazzez et al. [56]	analytical			

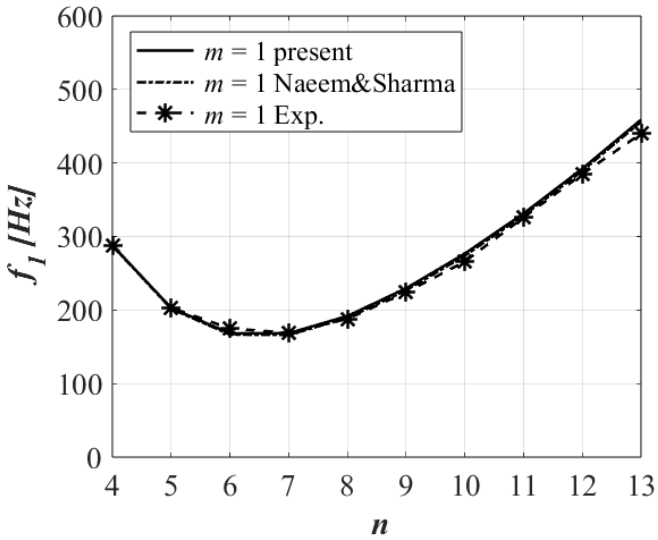

Figure 4. Comparison between the present model, Naeem and Sharma's model [50], and experimental data from Sewall and Neumann [15] (Exp.) for $m = 1$.

A comparison with the results reported by Pellicano [29] is presented in Tables 13 and 14, and Figure 6 for an aluminium cylinder with two simply supported ends and two clamped ends, respectively. Pellicano's model assumes Chebyshev polynomials for eigenfunctions and requires a numerical technique for the resolution. Data were available for $m = 1$ and $5 \leq n \leq 12$ for the simply supported/simply supported cylinder and for $m = 1$ and $6 \leq n \leq 13$ for the clamped/clamped cylinder. The percentage error is assessed against the results of an FEM analysis performed by Pellicano. For the cylinder with two simply supported ends, the exact solution is also provided. In this case, the results of Pellicano's numerical method equal the exact solution; nonetheless, the present model shows a maximum error of only 0.92% for $n = 8$ against FEM and 1.76% for $n = 9$ against the exact solution. The error in the global minimum frequency for $n = 7$ is 0.73% against FEM and -0.06% against

the exact solution. Concerning the clamped/clamped cylinder, Table 14 shows that the present model has a maximum error of 6.04% for $n = 6$, where Pellicano's method has a maximum error of 1.02%; however, the error of the present model in the global minimum frequency for $n = 9$ equals 2.88%, while Pellicano has an error of 0.34%. The error is still good, given the greater simplicity of the proposed novel formulation.

Table 11. Comparison among the present model, Naeem and Sharma's model [50] (N&S), and experimental data from Sewall and Neumann [15] (Exp.) for $m = 1$ for an aluminium simply supported/simply supported cylinder. The error for the global minimum is underlined in bold; an asterisk indicates the maximum error.

n	f_1(Hz)			Error (%)	
	Present	N&S [50]	Exp. [15]	Present vs. Exp.	N&S vs. Exp.
4	288	288	287	0.35	0.21
5	203	202	203	−0.11	−0.57
6	168	167	175	−3.89	−4.81 *
7	168	166	169	**−0.36**	**−1.64**
8	192	189	188	2.00	0.67
9	229	227	224	2.45	1.29
10	277	274	266	4.04	3.03
11	331	329	326	1.63	0.80
12	392	389	385	1.87	1.17
13	459	456	440	4.30*	3.68

Table 12. Comparison between the present model and experimental data from Arnold and Warburton [11] (Exp.) for a steel simply supported/simply supported cylinder. The error for the global minimum is underlined in bold; an asterisk indicates the maximum error.

n	$m = 1$			$m = 2$			$m = 3$			$m = 4$		
	f_1(Hz)		Error (%)	f_1(Hz)		Error (%)	f_1(Hz)		Error (%)	f_1(Hz)		Error (%)
	Present	Exp. [11]		Present	Exp. [11]		Present	Exp. [11]		Present	Exp. [11]	
2	1116	960	**16.22** *	2207	2070	6.62	3943	3725	5.86	5831	5270	10.64
3	2310	2130	8.44	2596	2420	7.29	3302	3130	5.49	4373	4180	4.62
4	4149	3985	4.11	4297	4130	4.04	4618	4430	4.25	5158	4950	4.21
5	6528	6400	2.01	6652	6500	2.34	6882	6700	2.72	7241	7030	3.01
6	9439	9270	1.83	9558	9370	2.00	9764	9570	2.03	10,068	9850	2.22

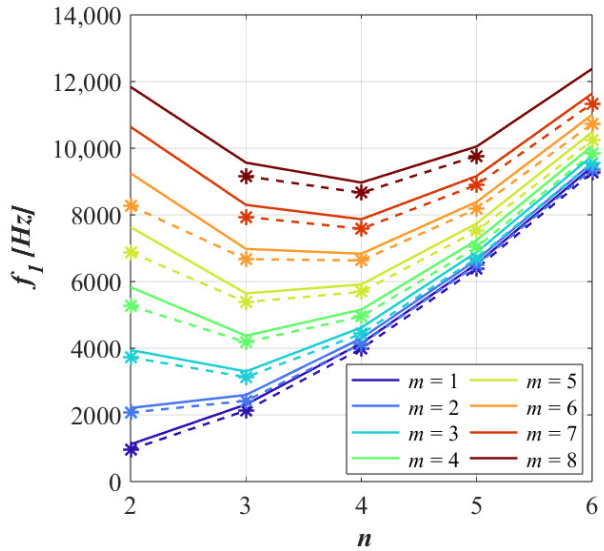

Figure 5. Comparison between the present model and the experimental results of Arnold and Warburton [11] for $m \leq 8$. The present results are represented by continuous lines; the experimental data are represented by X markers and dotted lines.

Table 13. Comparison between the present model and the results reported by Pellicano [29] for $m = 1$ for an aluminium simply supported/simply supported cylinder. The error for the global minimum is underlined in bold; an asterisk indicates the maximum error.

n	f_1 (Hz)				Error (%)		
	Present	**Pellicano [29]**	**Exact [29]**	**FEM [29]**	**Present vs. FEM**	**Pellicano vs. FEM**	**Present vs. Exact**
5	724	722	722	723	0.14	−0.06	0.20
6	556	553	553	554	0.39	−0.07	0.47
7	488	485	485	485	**0.73**	**−0.06**	**0.79**
8	494	490	490	490	0.92 *	−0.08	1.00
9	552	542	542	547	0.89	−0.86 *	1.76 *
10	643	637	637	638	0.74	−0.17	0.92
11	757	751	751	752	0.58	−0.21	0.79
12	888	882	882	885	0.41	−0.27	0.69

Table 14. Comparison between the present model and the results reported by Pellicano [29] for $m = 1$ for an aluminium clamped/clamped cylinder. The error for the global minimum is underlined in bold; an asterisk indicates the maximum error.

n	f_1 (Hz)			Error (%)	
	Present	**Pellicano [29]**	**FEM [29]**	**Present vs. FEM**	**Pellicano vs. FEM**
6	986	940	930	6.04 *	1.02 *
7	814	782	775	5.02	0.88
8	725	702	697	3.96	0.63
9	705	688	685	**2.88**	**0.34**
10	742	728	727	1.97	0.10
11	820	809	810	1.31	−0.06
12	930	921	922	0.87	−0.18
13	1063	1055	1057	0.61	−0.19

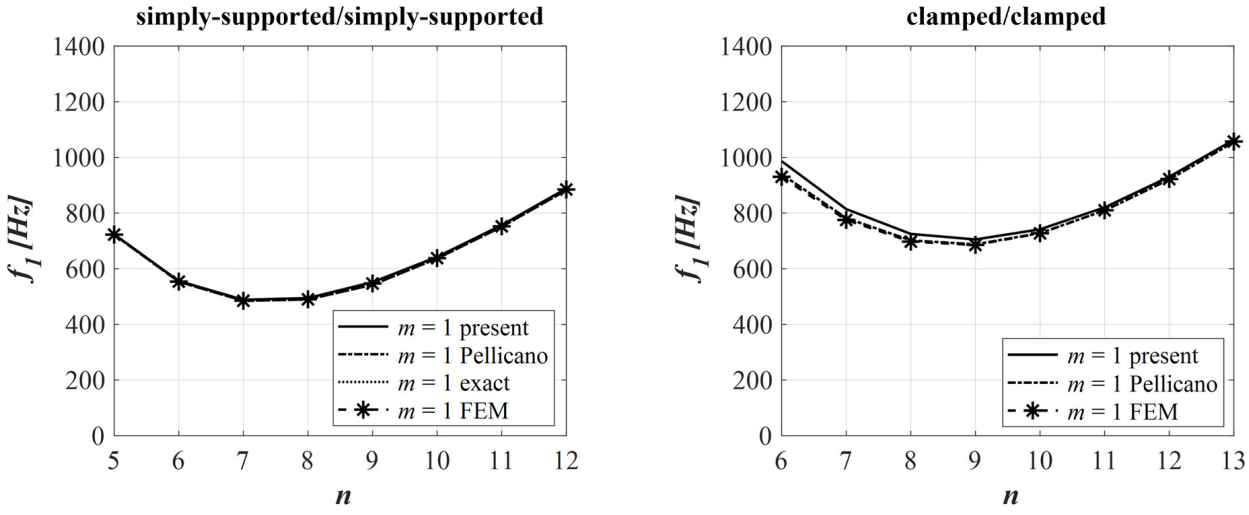

Figure 6. Comparison between the present model and Pellicano's numerical and FEM results [29] for $m = 1$.

Xuebin [54] used the wave propagation method and introduced the flexural vibrational mode of a beam to obtain a noniterative mathematical resolution based on a third-order equation. The natural frequencies for an aluminium clamped/clamped cylinder for $m = 1$, 3, 5, and $n \leq 10$ were assessed. Table 15 shows the comparison with the present model only for $m = 1$ for brevity, but complete results are shown in Figure 7. The error is assessed with respect to the results of an FEM analysis reported by Xuebin. The error in the global

minimum frequency for $n = 4$ is 8.22% for the present model against 1.16% for Xuebin. However, Xuebin's method shows a significant error for a low number of circumferential waves, achieving a maximum error of 36.19% for $n = 1$, more than three times higher than the maximum error of the present model equal to 10.04%. Moreover, the calculation of the coefficients of the third-order equation underpinning Xuebin's approach is rather convoluted in comparison to the present approximated model.

Table 15. Comparison between the present model and the results reported by Xuebin [54] for $m = 1$ for an aluminium clamped/clamped cylinder. The error for the global minimum is underlined in bold; an asterisk indicates the maximum error.

n	f_1(Hz)			Error (%)	
	Present	**Xuebin [54]**	**FEM [54]**	**Present vs. FEM**	**Xuebin vs. FEM**
1	1328	1644	1207	10.04 *	36.19 *
2	680	760	632	7.62	20.17
3	393	407	368	6.70	10.54
4	295	276	273	**8.22**	**1.16**
5	320	296	291	9.92	1.84
6	416	382	378	9.92	0.85
7	552	507	504	9.43	0.49
8	715	658	656	8.98	0.31
9	903	833	831	8.64	0.18
10	1114	1029	1028	8.38	0.08

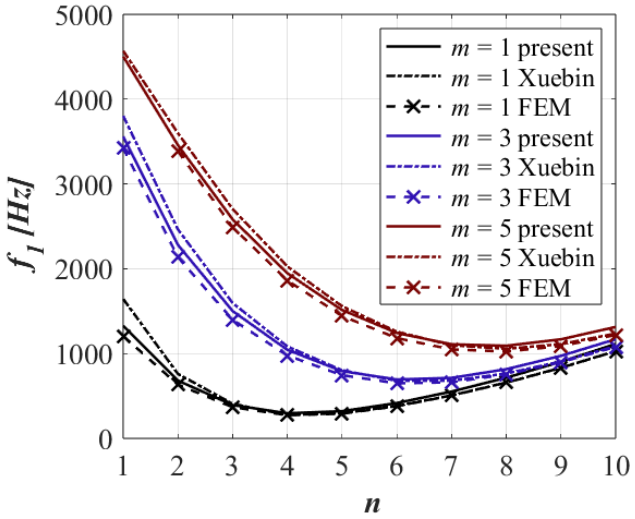

Figure 7. Comparison between the present model and Xuebin's analytical and FEM results [54] for $m = 1$, 3, and 5.

The last comparison is with the experimental data of Koval and Cranch [16], the analytical closed-form approaches of Wang and Lai [53] and Moazzez et al. [56], the exact solution of Xing et al. [33] numerically evaluated, and the FEM results discussed in Section 4.2. Wang and Lai used a direct formula derived from the free vibrations of an infinite-length cylinder. Moazzez et al. used a cascaded algebraic resolution of a third-order equation, presented by Cammalleri and Costanza in [46], that distinguishes different coefficients for even and odd numbers of transverse half-waves. Xing et al. used the Donnell–Mushtari equations without any other simplifying assumption; thus, the solution is "exact" but assessed by Newton's iterative method. Table 16 lists the first natural frequency assessed for $m = 1$ and $n \leq 8$. The present method and the one used by Moazzez et al. are in very good agreement, showing a maximum error lower than 10% for $n = 1$ and an error of approximately 3% in the global minimum frequency for

$n = 6$. The "exact" solution of Xing et al. shows the least error with respect to the FEM and experimental data. Against FEM, the maximum error against FEM of Xing et al. is −3.97% for $n = 2$, while the error in the global minimum frequency is −0.02%. Nonetheless, the higher error of the present model in comparison with Xing et al. is still acceptable, given the straightforward practice use of the present method that requires neither any initial guess frequencies nor a convergence analysis of the solving algorithm, unlike Xing et al. The approximated formula proposed by Wang and Lai is the less accurate, especially for lower n. It has a maximum error against FEM of 39.47% for $n = 1$ and an error in the global minimum frequency of 2.59%. Figure 8 shows the available first natural frequencies of the models under considerations for $m \leq 4$. Moazzez's results were excluded from the graphical comparison because they are almost the same as those obtained by the present model.

Table 16. Comparison among the present model and the results of Koval and Cranch [16] (Exp.), Wang and Lai [53] (W&L), Moazzez et al. [56], and Xing et al. [33] for $m = 1$ for a steel clamped/clamped cylinder. The error against FEM for the global minimum is underlined in bold; an asterisk indicates the maximum error.

n	f_1 (Hz)						Error (%)					
	Present	Moazzez [56]	W&L [53]	Xing [33]	Exp. [16]	FEM	Present/ Moazzez vs. FEM	W&L vs. FEM	Xing vs. FEM	Present/ Moazzez vs. Exp.	W&L vs. Exp.	Xing vs. Exp.
1	3788	3790	4811	3425	-	3450	9.82 *	39.47 *	−0.71	-	-	-
2	2084	2085	2452	1917	-	1996	4.40	22.84	−3.97 *	-	-	-
3	1233	1234	1356	1154	1025	1185	4.09	14.44	−2.61	20.33 *	32.29 *	12.59 *
4	806	807	847	764	700	769	4.79	10.07	−0.71	15.19	21.00	9.14
5	605	605	615	580	559	581	4.11	5.83	−0.19	8.23	10.02	3.76
6	555	555	552	538	525	538	**3.05**	**2.59**	**−0.02**	**5.62**	**5.14**	**2.48**
7	611	611	605	598	587	600	1.88	0.83	−0.34	4.14	3.07	1.87
8	736	736	728	723	720	729	0.97	−0.13	−0.81	2.22	1.11	0.42

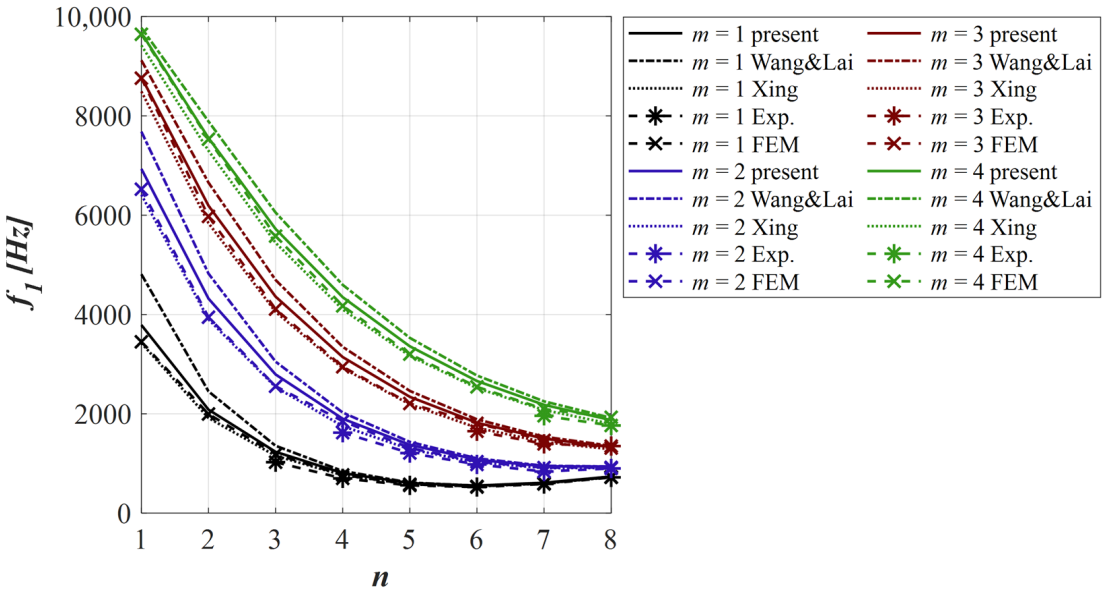

Figure 8. Comparison among the present model, the analytical closed-form approaches of Wang and Lai [53], the numerical solution of Xing et al. [33], the experimental data of Koval and Cranch [16] (Exp.), and FEM results.

Overall, the comparison presented in this section suggests that the numerical methods achieve more accurate results, especially with two clamped edges, but at the expense of fast usability. On the contrary, the present approximated model offers a swift, straightforward mathematical treatment which leads to satisfactory accuracy, especially if compared to other

analytical methods that sometimes fail for a low number of circumferential waves. The error for the global minimum frequency is generally much lower than 10%. Hence, the practical interest of the proposed approach is significant, given that its ease of use is hard to find in the relevant literature, especially for cylinders with one or two clamped ends. Moreover, it should be noted that, for a given absolute difference, the percentage error is higher for lower frequencies because of its own definition. Indeed, the graphical comparisons of Figures 4–8 show that the trend of the results obtained by the novel approximated model is in good agreement with FEM and experimental data, even when the percentage error in the global minimum is numerically higher.

When assessing the outcomes of the above comparisons, it should be considered that they may have been affected by potential errors in the results chosen as the benchmark. For instance, the fact that the frequencies resulting from experimental data are often lower than those numerically or analytically assessed suggests that the stiffness of the experimental set-up is lower than those theoretically predicted. Also, potential measurement errors may have occurred. Similarly, the goodness of the results of FEM analysis is strictly dependent on the mesh quality and elements number and type. Therefore, the errors of the present model are widely acceptable within the unavoidable uncertainty range of any engineering problem.

5. Conclusions

This paper proposed a novel procedure to study the free vibrations of an isotropic circular cylindrical shell under different boundary conditions.

The cylinder equations of motion of Donnell–Mushtari's shell theory were introduced in the principle of virtual work. The normalisation of the resulting system to the cylinder length and the introduction of the eigenfunction of a beam as constrained as the cylinder led to a significant simplification of the mathematical treatment, which was reduced to the eigenvalue problem of a 3×3 matrix. In other words, the problem of the free vibrations of a continuous system was reduced to the straightforward definition of a dynamic matrix depending on the cylinder geometry, material, and end constraints, similarly to the modal analysis of discreet systems.

The natural frequencies for several simply supported/simply supported, clamped/clamped, and clamped/simply supported cylinders were assessed and compared to FEM results, experimental data available in the literature, and other numerical and analytical methods. The vibrational behaviour of the clamped/simply supported cylinder lies between the double-simply supported condition, which implies the lowest frequencies, and the double-clamped condition, which results in the highest frequencies. For the cylinder proposed as a case study, the comparison with the present model and FEM analysis showed very good accuracy for a cylinder with two simply supported ends, involving a maximum error of 2.07%. This error increases with one or two clamped ends up to 11.9% and 9.82%, respectively. Nonetheless, the error occurring for the global minimum frequency, the most potentially dangerous, is just 2.01%, 3.66%, and 3.05%, respectively.

To provide a broader insight into the model validity, an FEM simulation campaign proved that the maximum error of approximately 10% for any combination of m and n is achievable for a wide range of cylinder geometry for any considered end condition. Within the assessed validity range, the error for the global minimum frequency is approximately 5% only. Moreover, a literature comparison showed that the present model resulted in comparable or even higher accuracy than other approximated closed-form approaches available in the literature, while the "exact" methods relying on more cumbersome and time-consuming iterative and numerical techniques perform better, at the expense of usability and immediacy of the computing procedure. Therefore, in general, the level of accuracy is excellent, given that the exact solution of the free vibrations problem for the clamped-end constraints does not exist in a closed form. Thus, the practical interest of the present model is significant.

To conclude, the proposed novel model proved to be a reliable, easy-to-use tool suitable for the rapid esteem of natural frequencies of thin-walled cylinders subject to simply supported or clamped-end conditions. The main strength is the excellent trade-off between usability and accuracy, making it easily implementable also in the design stage without requiring a deep knowledge of the topic.

Author Contributions: Conceptualization, M.C.; methodology, M.C.; software, A.C.; validation, A.C. and M.C.; investigation, A.C.; writing—original draft preparation, A.C.; writing—review and editing, M.C. and A.C.; visualization, A.C.; supervision, M.C. All authors have read and agreed to the published version of the manuscript.

Funding: This research received no external funding.

Data Availability Statement: Not applicable.

Conflicts of Interest: The authors declare no conflict of interest.

Nomenclature

r	cylinder mean radius
A_x, A_s, A_z	displacements amplitude
D	bending stiffness of the cylindrical shell
$\overline{\overline{D}}$	cylinder dynamic matrix
E	Young's modulus
f_1, f_2, f_3	natural frequencies
$\mathcal{F}_m$	beam transverse waveform with m half-waves
h	cylinder thickness
k_x, k_s	changes in the curvature of the mid-surface of the cylinder
K	tensile stiffness of the cylindrical shell
l	cylinder length
m	number of transverse half-waves
M_x, M_{xs}, M_{sx}, M_s	moments per unit length
n	number of circumferential waves
N_x, N_{xs}, N_s, N_{sx}	in-plane normal and shear forces per unit length
Q_x, Q_s	transverse shear forces per unit length
z	radial coordinate
s	circumferential coordinate
t	time coordinate
u_x, u_s, u_z	components of displacement of a point on the cylinder mid-surface
W	virtual work
x	axial coordinate
X	axial coordinate normalised to the cylinder length
R	mean radius normalised to the cylinder length
γ_{xs}	in-plane shear strain
ε_x, ε_s	normal strains
H	thickness normalised to the cylinder length
θ	angular circumferential coordinate
ν	Poisson's ratio
ρ	density
τ	cylinder mid-surface twist
ω_1, ω_2, ω_3	natural circular frequency

Appendix A

Table A1. Natural frequencies for a cylinder with two simply supported ends for $m \leq 4$ and $n \leq 14$ ($r = 76$ mm, $l = 305$ mm, $h = 0.254$ mm, $\rho = 7833$ kg/m^3, $E = 207$ kN/mm^2, $\nu = 0.3$). The minimum values of the first frequency f_1 for a given m are underlined. The global minimum frequency is highlighted in bold.

n	m = 1			m = 2			m = 3			m = 4		
	f_1 (Hz)	f_2 (Hz)	f_3 (Hz)	f_1(Hz)	f_2(Hz)	f_3(Hz)	f_1(Hz)	f_2(Hz)	f_3(Hz)	f_1(Hz)	f_2(Hz)	f_3(Hz)
1	2886	10,009	17,209	6445	14,059	21,944	8556	17,890	29,228	9527	22,354	37,344
2	1265	14,889	26,403	3677	18,061	29,947	5821	21,647	35,508	7344	25,581	42,338
3	656	20,923	36,632	2178	23,194	39,414	3896	26,222	43,820	5413	29,712	49,482
4	423	27,319	47,298	1396	29,012	49,558	2681	31,491	53,176	3986	34,518	57,937
5	**372**	33,847	58,183	985	35,177	60,072	1931	37,225	63,123	2994	39,833	67,200
6	431	40,433	69,190	792	41,523	70,807	1477	43,249	73,434	2323	45,509	76,983
7	551	47,048	80,272	751	47,971	81,681	1227	49,455	83,983	1884	51,434	87,115
8	705	53,681	91,403	819	54,481	92,649	1132	55,780	94,694	1626	57,533	97,491
9	887	60,325	102,566	956	61,031	103,683	1158	62,184	105,520	1516	63,753	108,044
10	1092	66,976	113,753	1139	67,607	114,764	1272	68,644	116,431	1526	70,063	118,728
11	1320	73,632	124,958	1355	74,203	125,881	1449	75,144	127,405	1630	76,438	129,511
12	1570	80,291	136,175	1599	80,814	137,024	1670	81,675	138,428	1803	82,863	140,371
13	1842	86,954	147,403	1867	87,434	148,189	1924	88,228	149,490	2028	89,327	151,293
14	2135	93,618	158,639	2159	94,063	159,370	2208	94,800	160,582	2292	95,821	162,263

Table A2. Natural frequencies for a cylinder with two clamped ends for $m \leq 4$ and $n \leq 14$ ($r = 76$ mm, $l = 305$ mm, $h = 0.254$ mm, $\rho = 7833$ kg/m^3, $E = 207$ kN/mm^2, $\nu = 0.3$). The minimum values of the first frequency f_1 for a given m are underlined. The global minimum frequency is highlighted in bold.

n	m = 1			m = 2			m = 3			m = 4		
	f_1(Hz)	f_2(Hz)	f_3(Hz)	f_1(Hz)	f_2(Hz)	f_3(Hz)	f_1(Hz)	f_2(Hz)	f_3(Hz)	f_1(Hz)	f_2(Hz)	f_3(Hz)
1	3788	15,184	20,252	6933	16,670	27,457	8781	19,735	35,709	9670	23,865	44,181
2	2084	20,428	27,371	4320	22,406	32,787	6192	25,054	39,893	7555	28,322	47,661
3	1233	25,548	37,098	2793	27,790	40,930	4360	30,509	46,555	5723	33,468	53,269
4	806	31,118	47,592	1901	33,239	50,501	3142	35,940	54,947	4348	38,784	60,588
5	605	37,026	58,396	1375	38,930	60,735	2342	41,481	64,358	3360	44,207	69,108
6	**555**	43,150	69,358	1077	44,843	71,312	1821	47,195	74,356	2661	49,768	78,415
7	611	49,414	80,410	943	50,924	82,089	1500	53,074	84,708	2181	55,477	88,235
8	736	55,773	91,520	938	57,129	92,991	1335	59,094	95,289	1873	61,327	98,400
9	903	62,197	102,668	1027	63,425	103,977	1300	65,225	106,023	1711	67,299	108,803
10	1102	68,670	113,844	1183	69,789	115,022	1369	71,446	116,866	1672	73,373	119,377
11	1326	75,177	125,039	1383	76,205	126,111	1513	77,736	127,788	1736	79,532	130,078
12	1574	81,712	136,250	1618	82,661	137,233	1714	84,082	138,771	1879	85,760	140,873
13	1845	88,268	147,471	1881	89,149	148,379	1956	90,474	149,800	2083	92,046	151,743
14	2138	94,841	158,702	2170	95,662	159,545	2231	96,903	160,865	2334	98,380	162,671

Table A3. Natural frequencies for a clamped/simply supported cylinder for $m \leq 4$ and $n \leq 14$ ($r = 76$ mm, $l = 305$ mm, $h = 0.254$ mm, $\rho = 7833$ kg/m^3, $E = 207$ kN/mm^2, $\nu = 0.3$). The minimum values of the first frequency f_1 for a given m are underlined. The global minimum frequency is highlighted in bold.

n	m = 1			m = 2			m = 3			m = 4		
	f_1(Hz)	f_2(Hz)	f_3(Hz)	f_1(Hz)	f_2(Hz)	f_3(Hz)	f_1(Hz)	f_2(Hz)	f_3(Hz)	f_1(Hz)	f_2(Hz)	f_3(Hz)
1	3485	12,713	17,907	6720	15,633	24,262	8676	18,943	32,238	9603	23,182	40,619
2	1737	17,084	26,746	4040	20,310	31,068	6026	23,497	37,427	7457	27,075	44,796
3	957	22,609	36,848	2512	25,367	40,048	4149	28,392	45,006	5580	31,674	51,192
4	609	28,655	47,454	1661	30,930	49,977	2928	33,644	53,962	4180	36,663	59,134
5	**476**	34,944	58,305	1183	36,844	60,380	2146	39,232	63,687	3187	41,975	68,072
6	482	41,360	69,290	932	42,979	71,048	1653	45,081	73,865	2499	47,559	77,648
7	574	47,851	80,357	842	49,256	81,879	1364	51,119	84,329	2037	53,358	87,643
8	717	54,387	91,476	873	55,627	92,818	1232	57,293	94,982	1751	59,323	97,925
9	893	60,955	102,631	988	62,063	103,829	1226	63,566	105,766	1613	65,417	108,410
10	1096	67,544	113,812	1158	68,545	114,894	1318	69,912	116,646	1598	71,609	119,044
11	1322	74,150	125,011	1368	75,062	125,997	1479	76,314	127,596	1681	77,879	129,788
12	1572	80,767	136,224	1607	81,605	137,130	1690	82,760	138,599	1840	84,209	140,619
13	1843	87,393	147,448	1874	88,168	148,286	1939	89,239	149,645	2054	90,588	151,516
14	2137	94,027	158,680	2164	94,747	159,459	2219	95,745	160,724	2312	97,006	162,466

Table A4. Displacement amplitudes' ratios for a cylinder with two simply supported ends for $m \leq 4$ and $n \leq 7$ ($r = 76$ mm, $l = 305$ mm, $h = 0.254$ mm, $\rho = 7833$ kg/m^3, $E = 207$ kN/mm^2, $\nu = 0.3$).

n	m = 1						m = 2					
	f_1		f_2		f_3		f_1		f_2		f_3	
	A_x/A_z	A_s/A_z	A_x/A_z	A_s/A_z	A_x/A_z	A_s/A_z	A_x/A_z	A_s/A_z	A_x/A_z	A_s/A_z	A_x/A_z	A_s/A_z
1	0.098	1.01	0.71	0.31	0.20	1.18	0.017	0.72	0.21	1.18	0.36	1.72
2	0.045	0.51	1.28	0.84	0.22	2.15	0.021	0.48	0.40	1.38	0.29	2.60
3	0.024	0.34	2.28	1.37	0.23	3.12	0.016	0.34	0.66	1.73	0.27	3.47
4	0.014	0.25	3.70	1.90	0.24	4.10	0.011	0.25	1.02	2.15	0.26	4.38
5	0.0094	0.20	5.52	2.41	0.24	5.08	0.0080	0.20	1.48	2.61	0.26	5.32
6	0.0067	0.17	7.76	2.93	0.24	6.07	0.0059	0.17	2.03	3.09	0.25	6.27
7	0.0049	0.14	10.40	3.44	0.25	7.06	0.0045	0.14	2.69	3.57	0.25	7.23
n	m = 3						m = 4					
	f_1		f_2		f_3		f_1		f_2		f_3	
	A_x/A_z	A_s/A_z	A_x/A_z	A_s/A_z	A_x/A_z	A_s/A_z	A_x/A_z	A_s/A_z	A_x/A_z	A_s/A_z	A_x/A_z	A_s/A_z
1	0.0014	0.42	0.14	2.45	0.52	2.25	0.0037	0.24	0.13	4.42	0.62	2.60
2	0.0079	0.39	0.24	2.12	0.37	3.21	0.0021	0.30	0.18	3.13	0.46	3.83
3	0.0091	0.31	0.36	2.26	0.31	4.00	0.0046	0.27	0.25	2.97	0.37	4.62
4	0.0078	0.25	0.52	2.56	0.29	4.82	0.0050	0.23	0.35	3.11	0.33	5.38
5	0.0063	0.20	0.73	2.94	0.28	5.69	0.0046	0.20	0.46	3.38	0.30	6.18
6	0.0050	0.17	0.97	3.36	0.27	6.59	0.0039	0.17	0.60	3.73	0.29	7.03
7	0.0040	0.15	1.27	3.80	0.26	7.52	0.0033	0.14	0.77	4.12	0.28	7.90

Table A5. Displacement amplitudes' ratios for a cylinder with two clamped ends for $m \leq 4$ and $n \leq 7$ ($r = 76$ mm, $l = 305$ mm, $h = 0.254$ mm, $\rho = 7833$ kg/m^3, $E = 207$ kN/mm^2, $\nu = 0.3$).

	$m = 1$						$m = 2$					
n	f_1		f_2		f_3		f_1		f_2		f_3	
	A_x/A_z	A_s/A_z	A_x/A_z	A_s/A_z	A_x/A_z	A_s/A_z	A_x/A_z	A_s/A_z	A_x/A_z	A_s/A_z	A_x/A_z	A_s/A_z
1	0.026	0.91	0.22	1.02	0.88	1.41	0.0057	0.64	0.097	1.52	0.87	1.92
2	0.022	0.49	0.89	1.55	0.41	2.25	0.011	0.45	0.27	1.94	0.52	2.83
3	0.015	0.33	1.85	1.94	0.32	3.17	0.010	0.32	0.54	2.31	0.38	3.62
4	0.011	0.25	3.06	2.35	0.28	4.13	0.0082	0.25	0.88	2.68	0.32	4.48
5	0.0078	0.20	4.57	2.79	0.27	5.11	0.0064	0.20	1.30	3.07	0.29	5.39
6	0.0058	0.17	6.38	3.25	0.26	6.09	0.0050	0.17	1.79	3.49	0.28	6.33
7	0.0045	0.14	8.52	3.71	0.26	7.08	0.0040	0.14	2.36	3.93	0.27	7.28
	$m = 3$						$m = 4$					
n	f_1		f_2		f_3		f_1		f_2		f_3	
	A_x/A_z	A_s/A_z	A_x/A_z	A_s/A_z	A_x/A_z	A_s/A_z	A_x/A_z	A_s/A_z	A_x/A_z	A_s/A_z	A_x/A_z	A_s/A_z
1	0.0014	0.38	0.077	2.63	0.91	2.27	0.0026	0.23	0.077	4.46	0.92	2.51
2	0.0042	0.37	0.16	2.55	0.62	3.45	0.0011	0.28	0.12	3.45	0.69	3.99
3	0.0057	0.30	0.29	2.81	0.45	4.22	0.0030	0.26	0.20	3.45	0.52	4.86
4	0.0055	0.24	0.45	3.12	0.37	4.99	0.0035	0.22	0.30	3.65	0.42	5.60
5	0.0048	0.20	0.65	3.47	0.33	5.82	0.0035	0.19	0.41	3.93	0.37	6.36
6	0.0041	0.17	0.89	3.84	0.30	6.69	0.0032	0.16	0.55	4.26	0.33	7.17
7	0.0034	0.14	1.16	4.24	0.29	7.60	0.0028	0.14	0.71	4.62	0.31	8.02

Table A6. Displacement amplitudes' ratios for a clamped/simply supported cylinder for $m \leq 4$ and $n \leq 7$ ($r = 76$ mm, $l = 305$ mm, $h = 0.254$ mm, $\rho = 7833$ kg/m^3, $E = 207$ kN/mm^2, $\nu = 0.3$).

	$m = 1$						$m = 2$					
n	f_1		f_2		f_3		f_1		f_2		f_3	
	A_x/A_z	A_s/A_z	A_x/A_z	A_s/A_z	A_x/A_z	A_s/A_z	A_x/A_z	A_s/A_z	A_x/A_z	A_s/A_z	A_x/A_z	A_s/A_z
1	0.051	0.95	0.53	0.72	0.31	1.25	0.0096	0.68	0.15	1.39	0.56	1.82
2	0.033	0.50	1.13	1.13	0.27	2.19	0.0152	0.46	0.35	1.68	0.37	2.70
3	0.020	0.34	2.02	1.58	0.26	3.15	0.0128	0.33	0.61	2.01	0.31	3.54
4	0.013	0.25	3.24	2.06	0.25	4.12	0.0097	0.25	0.96	2.39	0.28	4.43
5	0.0088	0.20	4.81	2.55	0.25	5.10	0.0072	0.20	1.38	2.82	0.27	5.35
6	0.0063	0.17	6.73	3.04	0.25	6.08	0.0055	0.17	1.90	3.27	0.26	6.30
7	0.0048	0.14	9.00	3.53	0.25	7.07	0.0043	0.14	2.51	3.73	0.26	7.26
	$m = 3$						$m = 4$					
n	f_1		f_2		f_3		f_1		f_2		f_3	
	A_x/A_z	A_s/A_z	A_x/A_z	A_s/A_z	A_x/A_z	A_s/A_z	A_x/A_z	A_s/A_z	A_x/A_z	A_s/A_z	A_x/A_z	A_s/A_z
1	0.0015	0.40	0.10	2.54	0.70	2.27	0.0031	0.24	0.10	4.42	0.76	2.55
2	0.0057	0.38	0.20	2.36	0.48	3.33	0.0015	0.29	0.15	3.31	0.56	3.92
3	0.0072	0.31	0.33	2.55	0.37	4.10	0.0037	0.27	0.23	3.22	0.44	4.74
4	0.0066	0.24	0.49	2.84	0.32	4.90	0.0042	0.23	0.32	3.39	0.37	5.48
5	0.0055	0.20	0.69	3.19	0.30	5.75	0.0040	0.19	0.44	3.65	0.33	6.27
6	0.0045	0.17	0.93	3.58	0.28	6.64	0.0035	0.17	0.58	3.98	0.31	7.09
7	0.0037	0.14	1.21	4.01	0.27	7.56	0.0030	0.14	0.74	4.36	0.29	7.96

References

1. Hemmer, M.; Van Khang, H.; Robbersmyr, K.G.; Waag, T.I.; Meyer, T.J.J. Fault Classification of Axial and Radial Roller Bearings Using Transfer Learning through a Pretrained Convolutional Neural Network. *Designs* **2018**, *2*, 56. [CrossRef]
2. Awada, A.; Younes, R.; Ilinca, A. Optimized Active Control of a Smart Cantilever Beam Using Genetic Algorithm. *Designs* **2022**, *6*, 36. [CrossRef]

3. Love, A.E.H. The Small Free Vibrations and Deformation of a Thin Elastic Shell. *Philos. Trans. R. Soc. Lond.* **1888**, *179*, 491–546. [CrossRef]
4. Flügge, W. *Stresses in Shells*; Springer: Berlin/Heidelberg, Germany, 1962; ISBN 3662010283.
5. Timoshenko, S.; Woinowsky-Krieger, S. *Theory of Plates and Shells*; McGraw Hill: New York, NY, USA, 1959; Volume 2.
6. Sanders, J.L., Jr. *An Improved First-Approximation Theory for Thin Shells*; US Government Printing Office: Washington, DC, USA, 1959; p. 1.
7. Reissner, E. A New Derivation of the Equations for the Deformation of Elastic Shells. *Am. J. Math.* **1941**, *63*, 177. [CrossRef]
8. Donnell, L.H. *Beams, Plates and Shells*; McGraw-Hill: New York, NY, USA, 1976; ISBN 0070175934.
9. Mushtari, K.M. Certain Generalizations of the Theory of Thin Shells. *Izv. Fiz. Mat. Ob-va. Pri Kaz. Un-te* **1938**, *11*, 28–56.
10. Leissa, A.W. *Vibration of Shells*; Scientific and Technical Information Office, National Aeronautics and Space Administration: Washington, DC, USA, 1973; Volume 288.
11. Arnold, R.N.; Warburton, G.B. Flexural Vibrations of the Walls of Thin Cylindrical Shells Having Freely Supported Ends. *Proc. R. Soc. Lond. Ser. A Math. Phys. Sci.* **1949**, *197*, 238–256. [CrossRef]
12. Warburton, G.B. Vibration of Thin Cylindrical Shells. *J. Mech. Eng. Sci.* **1965**, *7*, 399–407. [CrossRef]
13. Strutt, J.W.; Rayleigh, J.W.S.B. *The Theory of Sound*; Macmillan: New York, NY, USA, 1894; Volume 1.
14. Arnold, R.N.; Warburton, G.B. The Flexural Vibrations of Thin Cylinders. *Proc. Inst. Mech. Eng.* **1953**, *167*, 62–80. [CrossRef]
15. Sewall, J.L.; Naumann, E.C. *An Experimental and Analytical Vibration Study of Thin Cylindrical Shells with and without Longitudinal Stiffeners*; National Aeronautic and Space Administration: Washington, DC, USA, 1968; Volume 4705.
16. Koval, L.R.; Cranch, E.T. On the Free Vibration of Thin Cylindrical Shells Subjected to an Initial Static Torque. *Proc. 4th U.S. Natl. Congr. Appl. Mech.* **1962**, *1*, 107–117.
17. Smith, B.L.; Haft, E.E. Natural Frequencies of Clamped Cylindrical Shells. *AIAA J.* **1968**, *6*, 720–721. [CrossRef]
18. Sharma, C.B.; Johns, D.J. Vibration Characteristics of a Clamped-Free and Clamped-Ring-Stiffened Circular Cylindrical Shell. *J. Sound Vib.* **1971**, *14*, 459–474. [CrossRef]
19. Sharma, C.B. Free Vibrations of Clamped-Free Circular Cylinders. *Thin-Walled Struct.* **1984**, *2*, 175–193. [CrossRef]
20. Blevins, R.D. *Formulas for Natural Frequency and Mode Shape*; Van Nostrand Reinhold Co.: New York, NY, USA, 1979.
21. Soedel, W. *Vibrations of Shells and Plates*, 3rd ed.; Marcel Dekker: New York, NY, USA, 2004.
22. El-Mously, M. Fundamental Natural Frequencies of Thin Cylindrical Shells: A Comparative Study. *J. Sound Vib.* **2003**, *264*, 1167–1186. [CrossRef]
23. Forsberg, K. *A Review of Analytical Methods Used to Determine the Modal Characteristics of Cylindrical Shells*; NASA: Washington, DC, USA, 1966.
24. Santiago, J.M.; Wisniewski, H.L. Convergence of Finite Element Frequency Predictions for a Thin Walled Cylinder. *Comput. Struct.* **1989**, *32*, 745–759. [CrossRef]
25. Chung, H. Free Vibration Analysis of Circular Cylindrical Shells. *J. Sound Vib.* **1981**, *74*, 331–350. [CrossRef]
26. Bert, C.W.; Malik, M. Free Vibration Analysis of Thin Cylindrical Shells by the Differential Quadrature Method. *J. Press. Vessel Technol.* **1996**, *118*, 1–12. [CrossRef]
27. Loy, C.T.; Lam, K.Y.; Shu, C. Analysis of Cylindrical Shells Using Generalized Differential Quadrature. *Shock Vib.* **1997**, *4*, 193–198. [CrossRef]
28. Zhang, L.; Xiang, Y.; Wei, G.W. Local Adaptive Differential Quadrature for Free Vibration Analysis of Cylindrical Shells with Various Boundary Conditions. *Int. J. Mech. Sci.* **2006**, *48*, 1126–1138. [CrossRef]
29. Pellicano, F. Vibrations of Circular Cylindrical Shells: Theory and Experiments. *J. Sound Vib.* **2007**, *303*, 154–170. [CrossRef]
30. Xuebin, L. A New Approach for Free Vibration Analysis of Thin Circular Cylindrical Shell. *J. Sound Vib.* **2006**, *296*, 91–98. [CrossRef]
31. Khalili, S.M.R.; Davar, A.; Malekzadeh Fard, K. Free Vibration Analysis of Homogeneous Isotropic Circular Cylindrical Shells Based on a New Three-Dimensional Refined Higher-Order Theory. *Int. J. Mech. Sci.* **2012**, *56*, 1–25. [CrossRef]
32. Xie, X.; Jin, G.; Liu, Z. Free Vibration Analysis of Cylindrical Shells Using the Haar Wavelet Method. *Int. J. Mech. Sci.* **2013**, *77*, 47–56. [CrossRef]
33. Xing, Y.; Liu, B.; Xu, T. Exact Solutions for Free Vibration of Circular Cylindrical Shells with Classical Boundary Conditions. *Int. J. Mech. Sci.* **2013**, *75*, 178–188. [CrossRef]
34. Fakkaew, W.; Cole, M.O.T.; Chamroon, C. On the Vibrational Dynamics of Rotating Thin-Walled Cylinders: A Theoretical and Experimental Study Utilizing Active Magnetic Bearings. *Int. J. Mech. Sci.* **2019**, *163*, 105101. [CrossRef]
35. Rawat, A.; Matsagar, V.A.; Nagpal, A.K. Free Vibration Analysis of Thin Circular Cylindrical Shell with Closure Using Finite Element Method. *Int. J. Steel Struct.* **2020**, *20*, 175–193. [CrossRef]
36. Tang, D.; Wu, G.; Yao, X.; Wang, C. Free Vibration Analysis of Circular Cylindrical Shells with Arbitrary Boundary Conditions by the Method of Reverberation-Ray Matrix. *Shock Vib.* **2016**, *2016*, 3814693. [CrossRef]
37. Kumar, A.; Das, S.L.; Wahi, P. Effect of Radial Loads on the Natural Frequencies of Thin-Walled Circular Cylindrical Shells. *Int. J. Mech. Sci.* **2017**, *122*, 37–52. [CrossRef]
38. Tong, Z.Z.; Ni, Y.W.; Zhou, Z.H.; Xu, X.S.; Zhu, S.B.; Miao, X.Y. Exact Solutions for Free Vibration of Cylindrical Shells by a Symplectic Approach. *J. Vib. Eng. Technol.* **2018**, *6*, 107–115. [CrossRef]

39. Jia, J.; Lai, A.; Li, T.; Zhou, Z.; Xu, X.; Lim, C.W. A Symplectic Analytical Approach for Free Vibration of Orthotropic Cylindrical Shells with Stepped Thickness under Arbitrary Boundary Conditions. *Thin-Walled Struct.* **2022**, *171*, 108696. [CrossRef]
40. Borković, A.; Radenković, G.; Majstorović, D.; Milovanović, S.; Milašinović, D.; Cvijić, R. Free Vibration Analysis of Singly Curved Shells Using the Isogeometric Finite Strip Method. *Thin-Walled Struct.* **2020**, *157*, 107125. [CrossRef]
41. Li, H.; Pang, F.; Miao, X.; Gao, S.; Liu, F. A Semi Analytical Method for Free Vibration Analysis of Composite Laminated Cylindrical and Spherical Shells with Complex Boundary Conditions. *Thin-Walled Struct.* **2019**, *136*, 200–220. [CrossRef]
42. Liew, K.M.; Hu, Y.G.; Ng, T.Y.; Zhao, X. Dynamic Stability of Rotating Cylindrical Shells Subjected to Periodic Axial Loads. *Int. J. Solids Struct.* **2006**, *43*, 7553–7570. [CrossRef]
43. Rizzetto, F.; Jansen, E.; Strozzi, M.; Pellicano, F. Nonlinear Dynamic Stability of Cylindrical Shells under Pulsating Axial Loading via Finite Element Analysis Using Numerical Time Integration. *Thin-Walled Struct.* **2019**, *143*, 106213. [CrossRef]
44. Ng, T.Y.; Lam, K.Y.; Liew, K.M.; Reddy, J.N. Dynamic Stability Analysis of Functionally Graded Cylindrical Shells under Periodic Axial Loading. *Int. J. Solids Struct.* **2001**, *38*, 1295–1309. [CrossRef]
45. Weingarten, V.I. Free Vibration of Thin Cylindrical Shells. *Aiaa J.* **2012**, *2*, 717–722. [CrossRef]
46. Cammalleri, M.; Costanza, A. A Closed-Form Solution for Natural Frequencies of Thin-Walled Cylinders with Clamped Edges. *Int. J. Mech. Sci.* **2016**, *110*, 116–126. [CrossRef]
47. Cammalleri, M.; Castellano, A.; Abella, M. A Simple Tool to Forecast the Natural Frequencies of Thin-Walled Cylinders. *Mater. Res. Proc.* **2023**, *26*, 635–640. [CrossRef]
48. Yang, Y.; Wei, Y. A Unified Approach for the Vibration Analysis of Cylindrical Shells with General Boundary Conditions. *Acta Mech.* **2018**, *229*, 3693–3713. [CrossRef]
49. Sorge, F.; Cammalleri, M. On the Beneficial Effect of Rotor Suspension Anisotropy on Viscous-Dry Hysteretic Instability. *Meccanica* **2012**, *47*, 1705–1722. [CrossRef]
50. Naeem, M.N.; Sharma, C.B. Prediction of Natural Frequencies for Thin Circular Cylindrical Shells. *Proc. Inst. Mech. Eng. Part C J. Mech. Eng. Sci.* **2000**, *214*, 1313–1328. [CrossRef]
51. Qin, Z.; Chu, F.; Zu, J. Free Vibrations of Cylindrical Shells with Arbitrary Boundary Conditions: A Comparison Study. *Int. J. Mech. Sci.* **2017**, *133*, 91–99. [CrossRef]
52. Ji, M.; Inaba, K.; Triawan, F. Vibration Characteristics of Cylindrical Shells Filled with Fluid Based on First-Order Shell Theory. *J. Fluids Struct.* **2019**, *85*, 275–291. [CrossRef]
53. Wang, C.; Lai, J.C.S. Prediction of Natural Frequencies of Finite Length Circular Cylindrical Shells. *Appl. Acoust.* **2000**, *59*, 385–400. [CrossRef]
54. Xuebin, L. Study on Free Vibration Analysis of Circular Cylindrical Shells Using Wave Propagation. *J. Sound Vib.* **2008**, *311*, 667–682. [CrossRef]
55. Zhang, X.M.; Liu, G.R.; Lam, K.Y. Vibration Analysis of Thin Cylindrical Shells Using Wave Propagation Approach. *J. Sound Vib.* **2001**, *239*, 397–403. [CrossRef]
56. Moazzez, K.; Saeidi Googarchin, H.; Sharifi, S.M.H. Natural Frequency Analysis of a Cylindrical Shell Containing a Variably Oriented Surface Crack Utilizing Line-Spring Model. *Thin-Walled Struct.* **2018**, *125*, 63–75. [CrossRef]
57. Ramezani, H.; Mirzaei, M. Transient Elastodynamic Behavior of Cylindrical Tubes under Moving Pressures and Different Boundary Conditions. *Appl. Math. Model.* **2020**, *77*, 934–949. [CrossRef]